Manuscript Details

Manuscript number	ADWR_2019_440_R3
Title	Open channel flow within and above a layered vegetation: Experiments and first-order closure modeling
Article type	Research Paper

Abstract

Flow within vegetation characterized by non-uniform roughness density is drawing significant research work and it has remarkable relevance to a plethora of applications in eco-hydraulics including river restoration and flow in wetland and marshes. Following that, the mean longitudinal velocity profile in a two layered cylindrical vegetation system is studied using flume experiments and then new first-order closure model is derived for the same. Layer 1 represents the region close to the channel bottom where the flow experiences maximum drag due to the densely placed vegetation, while layer 2 represents the flow region above the short vegetation characterized by a smaller vegetation density. Considering the aforementioned arrangements, a new analytical model based on Reynolds-averaged closure principles is proposed to describe the vertical distribution of mean streamwise velocity in an open channel with two different vegetation densities. In the proposed model, the one-dimensional steady and planar-homogeneous momentum equation is used where the turbulent eddy viscosity is assumed to be linearly related to the local mean velocity. The proposed analytical model has been calibrated using experiments reported here in which vegetation is represented by using circular plastic cylinders of two different heights. The proposed model is further tested against published experiments with similar arrangements. In total, 22 different experimental conditions with distinct densities, rigidity, and flow depths have been analyzed. The Root Mean Square Error (RMSE) of the velocity comparisons is found to be less than 0.0342 m/s, which is par acceptable.

Keywords	Emergent vegetation, open channel flow, submerged vegetation, two layer vegetation, velocity profiles.

Corresponding Author	XIAONAN TANG
Corresponding Author's Institution	Xi'an Jiaotong-Liverpool University
Order of Authors	Hamidreza Rahimi, XIAONAN TANG, Prateek Kumar Singh, Ming Li, Sina Alaghmand
Suggested reviewers	Alireza Pourbakhtiar, Samad Emamgholizadeh, Songdong Shao, Alireza Farid Hosseini, Seyed Iman Saedi

Submission Files Included in this PDF

File Name [File Type]

ADWR4.Cover.Letter.30.1.docx [Cover Letter]

Review2.AWR_30.1.docx [Response to Reviewers]

ADWR.R4_updated2F.docx [Revised Manuscript with Changes Marked]

Highlights.docx [Highlights]

ADWR.R4_updated2F_no.docx [Manuscript File]

No conflicts_30.1.docx [Conflict of Interest]

AWR.Statement.docx [Author Statement]

To view all the submission files, including those not included in the PDF, click on the manuscript title on your EVISE Homepage, then click 'Download zip file'.

Research Data Related to this Submission

There are no linked research data sets for this submission. The following reason is given:
Data will be made available on request

Open channel flow within and above a layered vegetation: Experiments and first-order closure modeling

H.R. Rahimi [1], X. Tang [2*], P. Singh [3], M. Li[4], S. Alaghmand [5]

1 Department of Civil Engineering, Xi'an Jiaotong-Liverpool University, China
Hamidreza.rahimi@liverpool.ac.uk
2 Department of Civil Engineering, Xi'an Jiaotong-Liverpool University, China
Xiao.tang@xjtlu.edu.cn
3 Department of Civil Engineering, Xi'an Jiaotong-Liverpool University, China
P.singh@xjtlu.edu.cn
4 Department of Engineering, University of Liverpool, UK
M.li@liverpool.ac.uk
5 Department of Civil Engineering, Monash University, Australia
Sina.alaghmand@monash.edu.au

*Corresponding author.

Abstract

Flow within vegetation characterized by non-uniform roughness density is drawing significant research attention given its relevance to a plethora of applications in eco-hydraulics including river restoration, and flow in wetland and marshes. The focus here is on flume experiments and modeling of the mean longitudinal velocity profile in a two layered cylindrical vegetation system. Layer 1 represents the region close to the channel bottom where the flow experiences maximum drag due to the densely placed vegetation, while layer 2 represents the flow region above the short vegetation characterized by a smaller vegetation density. Considering the aforementioned arrangements, a new analytical model based on Reynolds-averaged closure principles is proposed to describe the vertical distribution of mean streamwise velocity in an open channel with two different vegetation densities. In the proposed model, the one-dimensional steady and planar-homogeneous momentum equation is used where the turbulent eddy viscosity is assumed to be linearly related to the local mean velocity. The proposed analytical model has been calibrated using experiments reported here

in which vegetation is represented by using circular plastic cylinders of two different heights. The proposed model is further tested against published experiments with similar arrangements. In total, 22 different experimental conditions with distinct densities, rigidity, and flow depths have been analyzed. The Root Mean Square Error (RMSE) of the velocity comparisons is found to be less than 0.0342 m/s, which is acceptable.

Keywords: Emergent vegetation, open channel flow, submerged vegetation, two layer vegetation, velocity profile.

Introduction

The hydrodynamics of free surface flow through and above vegetation is impacted by the presence of vegetation, which affects the velocity, boundary shear, Reynolds stress, and turbulence intensity (Nepf, 1999; Nepf and Vivoni, 2000; Lopez and Garcia 2001; Ghisalberti and Nepf, 2006; Poggi et al. 2004; Stoesser et al., 2010). Furthermore, flow induced through differential vegetation heights, densities and flow depth alters the overall roughness, which completely changes the physics of the flow. In addition, the complexity of flow manifolds, due to macro roughness, causes this type of flow no longer to be explained through a single global factor such as Manning's roughness coefficient.

Multiple mechanisms impact the flow description within vertically non-uniform canopies (Katul et al., 2011; Nikora et al., 2013; Huai et al., 2014). These multiple mechanism can be represented layer by layer to account for changes in roughness density, vegetation height, water level, and dominant vertical structures (Carollo et al., 2002; Huai et al., 2014; Tang & Ali, 2013; Tang, 2018a, 2019a-c; Singh et al., 2019a).

Previous methods describing the mean velocity profile employed the approaches based on solutions to the mean momentum equation that is subject to closure schemes for the total

stresses. The most problematic feature of the velocity profile is the shear layer at the top of vegetation, which is induced through gradient of velocity (Raupach et al., 1996). The turbulence produced in this region is governed by the mixing length and vertical turbulent transport of momentum from the overlying flow, with the negligible contribution from the pressure gradient. The effect of the shear length scale was found to be a function of the vegetation height and flow depth (Klopstra et al., 1996; Defina and Bixio, 2005; Tang, 2019a&c; Singh et al. 2019a).

Several studies and experiments (see Fig.1) have examined the submerged single layered flow with both flexible and rigid plant models (Poggi et al., 2004; Nikora et al., 2013; Okamoto and Nezu, 2013; Liu et al., 2010; Huai et al., 2014). However, only few studies have examined the two layered vegetation flow with tall vegetation being emergent i.e. $h_t > H$, where h_t is the height of the tall vegetation and H is the flow depth. This condition seems most realistic in case of real time scenarios, where the flow depth covers the small vegetation but the taller vegetation is emergent throughout the flow. Finally, momentum transport is mainly due to vertical turbulent exchange since the longitudinal advection can be insignificant in the lower vegetation zone (Fig. 1).

Using the mean longitudinal momentum balance equation subject to planar homogeneous, steady state conditions and further assuming bed and wall shear stresses to be negligible compared to the drag force imposed by the vegetation, a mathematical model is proposed and tested using new flume experiments.

This paper develops and evaluates a phenomenological model for estimating the vertical distribution of mean longitudinal velocity in the two layer vegetation with taller vegetation being emergent. Our experimental studies have shown that, the density of vegetation plays a

key role in capturing the inflection point and the mixing length over the short vegetation height. The flow is divided into two layers that are modelled independently by coupled through continuity and smoothness. The application of the proposed model was carried out in a condition where short dowels are fully submerged, but the tall ones are emergent. The first zone is the one that starts from the channel bed to the location near the top of short vegetation; the second zone is in between the top of short vegetation and the water surface. For the two zones, different parameters have been embedded in the proposed analytical equations to predict the flow velocity for the aforementioned condition. In addition, the performance of the proposed method was evaluated with 22 experimental data using root mean square (Banerjee et al., 2018; Tang, 2018b).

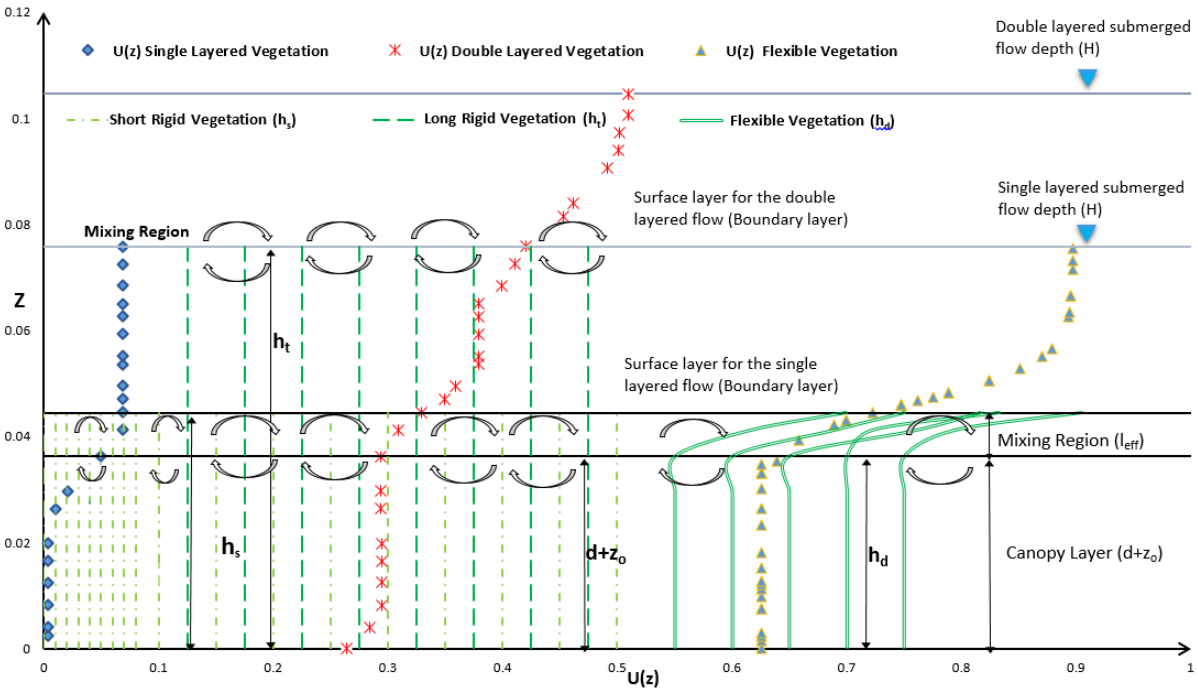

Figure 1. Schematic of the mean velocity profile through single (rigid and flexible) and two layered (rigid) vegetation with flow depth (H) for respective vegetation configuration. The mixing region and inflection point over the short (h_s), undeflected (h_d) and tall (h_t) vegetation are depicted with the vertical distribution of the longitudinal velocity U(z). The von-Karman street, mixing region and boundary layer in the profile can be found in $d+z_o$, l_{eff} and surface layer region, as shown in the conceptual model of vegetative flow within a straight channel respectively.

Theoretical background

Vegetation inside the channel could be either emergent or submerged. Experimental studies have shown that the vertical distribution of mean velocity in emergent conditions is almost uniform over the depth (Tsujimoto and Kitamura, 1990; Stone and Shen, 2002). On the other hand in submerged conditions, the vertical distribution of mean velocity follows an 'S-shaped' pattern with inflection over the zero plane displacement generally found near the top of the short vegetation (Kouwen et al., 1969; Temple, 1986; Ikeda and Kanazawa, 1996; Carollo et al. 2002). The previous analytical models proposed by Klopstra et al. (1996), Ghisalberti and Nepf (2004), Poggi et al. (2004), Defina and Bixio (2005), Kubrak et al. (2008), Huai et al. (2014) and Tang (2019c) are all based on the steady uniform momentum equation (Eq.1). The wall and bed boundary shear stresses are considered to be negligible in the vegetation column where drag induced forces are the primary resistance to the flow. Under those idealized conditions, the mean momentum balance is given by

$$\frac{1}{\rho}\frac{\partial \tau(z)}{\partial z} = F_v - gS_0, \tag{1}$$

where τ is the turbulent shear stress, ρ is the density of water, g is the gravitational acceleration, z is the vertical coordinate above the bed, S_0 is the bed slope, and F_v is the drag force per unit mass generated by the vegetation. Drag force can be defined by:

$$F_v = \begin{cases} \frac{1}{2}C_D a u^2, & z \le h \\ 0, & z > h \end{cases} \quad ; \quad a = mA_V, \tag{2}$$

where u is the velocity in the streamwise direction, h is the vegetation height, C_D is the vegetation drag coefficient, a is the vegetation density, m and A_V are the number of vegetation per unit area and the frontal area of vegetation per unit volume, respectively. In Eq. (1) the shear stress can be modeled through the Boussinesq hypothesis as:

$$\tau(z) = \rho \nu_t \frac{\partial u}{\partial z} = \rho \phi u(z) \frac{\partial u}{\partial z}, \tag{3}$$

where the total eddy viscosity v_t is defined as the product of local velocity scale and the characteristic length scale ϕ, which is assumed to be independent of vertical component z (Klopstra et al. 1997; Defina & Bixio, 2005). Meanwhile, it is worth noting that the local velocity u(z) here is chosen as a characteristic velocity for the eddy viscosity model in Eq. (3), which is one of different hypotheses for eddy viscosity models used in the literature. If distinct models are used, a different form of solution can result (e.g. Huai et al. 2014).

Inserting Eqs. (2) & (3) into Eq. (1) gives:

$$\phi \frac{\partial^2(u^2)}{\partial z^2} - aC_D u^2 + 2gS_0 = 0\,, \qquad (4)$$

Eq.(4) can be solved analytically for u^2 by providing the vegetation density a, drag coefficient C_D and eddy characteristic length scale ϕ with boundary conditions, which vary from datum to short vegetation height ($0 < z < h_s$) as layer 1 and from the short vegetation height to the free surface ($h_s < z < H$) as layer 2 (Fig. 2). The subsequent Eq. (4) is used to develop the new analytical model for the case of two layered vegetative flow with emergent tall vegetation. The closure of the proposed model is obtained through modelling parameters such as drag coefficient C_D and characteristic length scale ϕ, which will be discussed by acknowledging the physics of the flow with complete explanation and contextual background in a later section.

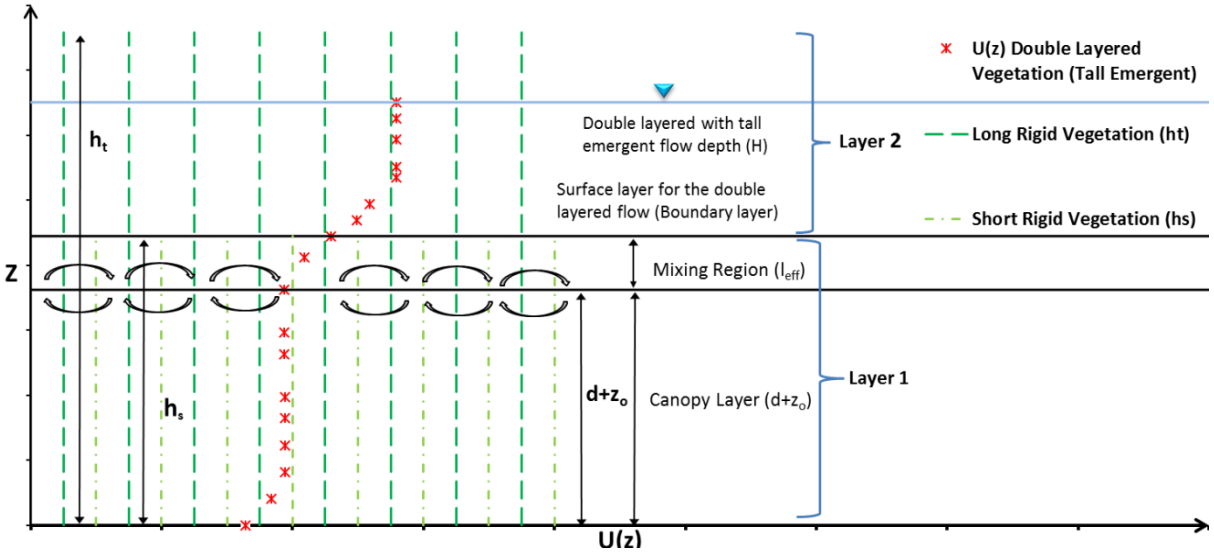

Figure 2. Two different layers of streamwise velocity in the vegetative flow for tall vegetation being emergent.

Previous models

Klopstra et al. (1997) proposed a model for single layered vegetation using Eq. (4) and boundary conditions such as $u_o = u|_{z=o} = \sqrt{\frac{2gS_o}{aC_D}}$, where negligible bed shear stress is considered with the local equilibrium between the gravity force and vegetation drag along with the condition for the boundary shear stress at the top of vegetation to be considered as $\tau_{z=h} = \rho g(H-h)S_o$. The symbols have usual meaning as mentioned earlier. The flow velocity in the vegetation layer is given by:

$$u_v = \sqrt{C_1 e^{-z\sqrt{2A}} + C_2 e^{z\sqrt{2A}} + u_{s0}^2} \qquad (0 < z < h), \tag{5}$$

where C_1 and C_2 are the integration constants, and u_{s0} is the characteristic constant flow velocity in non-submerged condition. The terms A, u_{so}, C_1 and C_2 are given as:

$$A = \frac{mdC_D}{2\emptyset}, \tag{6}$$

$$u_{s0} = \sqrt{\frac{2gS_o}{C_D md}}, \tag{7}$$

where d is the diameter of cylindrical vegetation. C_1 and C_2 can be determined to ensure that the upper and lower boundary conditions are satisfied. C_1 and C_2 in Eq. (5) are derived as Eqs. (8) & (9) using limiting boundary conditions and are given as:

$$C_1 = \frac{-2gS_o(H-h)}{\emptyset\sqrt{2A}(e^{h\sqrt{2A}} + e^{-h\sqrt{2A}})}, \tag{8}$$

$$C_2 = -C_1, \tag{9}$$

where h is the height of vegetation. The log law of Prandtl defined for the surface layer can be expressed as:

$$\frac{u}{u_*} = \frac{1}{\kappa} ln\left(\frac{z-(h-\delta_s)}{K_s}\right) \qquad (z \geq h), \tag{10}$$

where u_* is the shear velocity, κ is the von Karman constant taken as 0.4, K_s is the height of the virtual bed roughness of the surface layer, and δ_s is the vertical shift of the virtual zero

level of the logarithmic profile. By applying continuity and smoothness conditions on the mean velocity profile, parameters δ_s and K_s can be determined and are given as:

$$\delta_s = g\,\frac{1+\sqrt{1+\frac{4.E^2\kappa^2(H-h)}{g}}}{2.E^2\kappa^2}, \quad (11)$$

$$K_s = \delta_s e^{-F}, \quad (12)$$

where

$$E = \frac{\sqrt{2.A}\;C_3 e^{h\sqrt{2A}}}{2.\sqrt{C_3 e^{h\sqrt{2A}} + u_{v0}^2}}, \quad (13)$$

$$F = \frac{k\sqrt{C_3 e^{h\sqrt{2A}} + u_{v0}^2}}{\sqrt{g\,(H-(h-\delta_s))}}, \quad (14)$$

$$u_{v0} = \frac{u_{s0}}{\sqrt{S_o}}, \quad (15)$$

$$C_3 = \frac{C_2}{S_o}. \quad (16)$$

The velocity profile, inside and above the vegetation, is defined by Eq. (5) and (10), respectively, while all the limiting boundary conditions and the variables used in the equations can be found in Eqs. (6)-(9) and Eqs. (11)-(16), accordingly. Klopstra et al. (1997) found a relationship between ϕ and vegetation characteristic with flow depth as:

$$\phi = 0.0793\,h\,ln\frac{H}{h} - 0.0009 \quad \text{and} \quad \phi \geq 0.001. \quad (17)$$

Meijer and Van Velzen (1999) conducted an experimental study and applied Klopstra et al. (1997) model, which confirmed the applicability of the model for their set of data. However, they found out that the model for the mixing length parameter ϕ of Eq. (17) was not suitable for their datasets. Therefore, Meijer and Van Velzen (1999) gave a new model for the mixing length parameter (ϕ) by considering the same variables but with different curve fitting function. The fitting procedure to their data resulted in:

$$\phi = 0.0144\sqrt{Hh}. \quad (18)$$

Baptist et al. (2007) used the mixing-length concept to define the eddy viscosity v_t as:

$$v_t(z) = lk_t = c_p l\, u(z), \tag{19}$$

where l is defined as a characteristic mixing length that is found to be the function of the spatial arrangement of vegetation, k_t is the turbulent kinetic energy per unit mass, and c_p is the turbulence intensity that is defined as:

$$c_p = \frac{\left(\frac{1}{h}\right)\int_0^h \sqrt{h(z)dz}}{\left(\frac{1}{h}\right)\int_0^h \sqrt{u(z)dz}}\ . \tag{20}$$

Thus, Eq.(5) becomes as: as

$$u_v = \sqrt{u_{s0}^2 + ae^{z/L} + be^{-z/L}}, \tag{21}$$

$$u_{s0} = \sqrt{\frac{2gS_o}{C_D md}}, \tag{22}$$

$$L = \sqrt{\frac{C_p l}{C_D md}}\,. \tag{23}$$

where a and b are the integration constants. Eq. (21) comprises two different components, which can be labelled as near free surface component and near bed component. The first component is dealt with $ae^{z/L}$ while the latter one is $be^{-z/L}$. Therefore, the shape of the profile is determined by the values of integration constants a and b. In further analysis, constant value of b is found to be insignificant for estimating the vertical distribution of mean velocity in vegetation area. Fig. 3 shows that there is a decline in the velocity trend from the top of the vegetation downward, until the uniform flow velocity u_{s0} is reached.

Ultimately, the velocity profile through the vegetation is defined by:

$$u_v = \sqrt{S_o(u_{v0}^2 + a_v e^{z/L})}, \tag{24}$$

where

$$u_{v0} = \sqrt{\frac{2g}{C_D md}} \text{ and } a_v = \frac{2Lg\,(H-h)}{c_p l\, e^{\frac{h}{l}}}. \tag{25}$$

Baptist et al. (2007) also studied the velocity above vegetation and modeled it using the same logarithmic profile, where they tried to shift the inflection using a vertical asymptote called momentum absorption, δ_v or zero plane displacement, given by:

$$\frac{u}{u_*} = \frac{1}{\kappa} ln\left(\frac{z-\delta_v}{K_s}\right), \tag{26}$$

where the vertical position of the centroid of momentum absorption, δ_v, was calculated by Thom (1971) using the centroid method and is given as:

$$\delta_s = \frac{\int_0^h \frac{d\tau(z)}{dz} z dz}{\int_0^h \frac{d\tau(z)}{dz} dz}. \tag{27}$$

The boundary condition over the vegetation was used to compute the roughness height (K_s) so that the velocity profile through the vegetation, $u_v(z)$, is matched to the logarithmic profile of flow velocity $u_0(z)$. Thus, δ_s and K_s are given by:

$$\delta_s = h_v - L\left(1 - e^{-\frac{h}{l}}\right), \tag{28}$$

$$K_s = (h-\delta_s) e^{\left(-k\sqrt{\frac{2L}{c_p}\left(1+\frac{L}{H-h}\right)}\right)}. \tag{29}$$

Finally, the turbulence intensity, c_p, is approximated as:

$$c_p = \frac{1}{20}\frac{H-h}{l}. \tag{30}$$

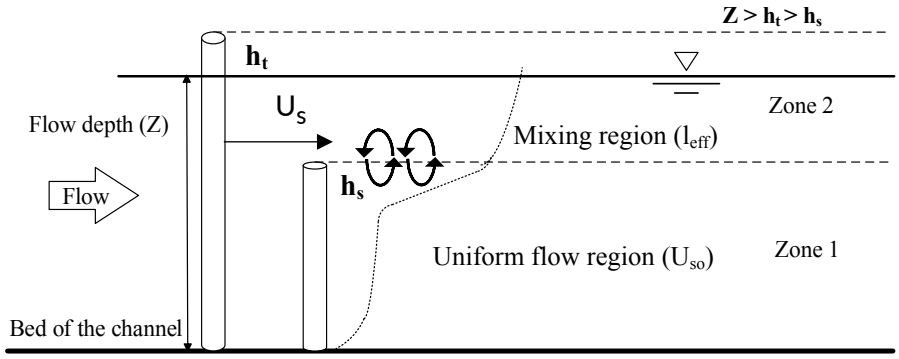

Figure 3. Illustration of flow with two-layer vegetation

To determine the overall streamwise velocity in submerged condition, an analytical model was established by Huthoff et al. (2007) using cylindrical dowels to represent vegetation with two different layers (Fig.4). The proposed model of Huthoff et al. (2007) is given in Eqs. (31) and (32) for the average velocity in the subsequent layers.

$$U_v = \sqrt{\frac{2bgS_o}{1+\frac{2b}{H}f}}, \quad \text{for emergent condition, } H \leq h \tag{31}$$

$$U_v = \sqrt{\frac{2bgS_o}{1+\frac{b}{32h}\left(\frac{K_s}{H}\right)^{1/3}}}, \quad \text{for submerged condition, } H \geq h \tag{32}$$

where f is the coefficient of bed resistance and b is defined by Belcher et al. (2003) as:

$$b = \frac{1}{C_D m d}. \tag{33}$$

Moreover, the average velocity in the surface layer can be scaled with l, the scaling length, and α, the transition exponent, as in Eq. (34):

$$\frac{U_s}{U_v} \sim \left(\frac{H-h}{l}\right)^{\frac{2}{3}\left[1-\left(\frac{H}{h}\right)^{-\alpha}\right]}. \tag{34}$$

Nezu and Sanjou (2008) assumed the three sub-zones in the vegetated region as, emergent zone ($0 \leq z \leq h_p$), mixing-layer zone ($h_p \leq z \leq h_{log}$), and log-law zone ($h_{log} \leq z \leq H$) as shown in Fig.4.

Wake effects from stem in the emergent zone (see Fig. 4) lead to a mean velocity profile that is vertically uniform as discussed elsewhere (Nezu and Sanjou, 2008). Comparing to some previous studies, this zone is similar to the ‘‘longitudinal exchange area’’ in which the vertical transport of momentum is considerably small (Nepf and Vivoni, 2000).

Nepf and Vivoni (2000) and Ghisalberti and Nepf (2006) designated the entire upper zone as the exchange zone, while Nezu and Sanjou (2008) divided it into two zones named as, the “mixing-layer” and “log-law”.

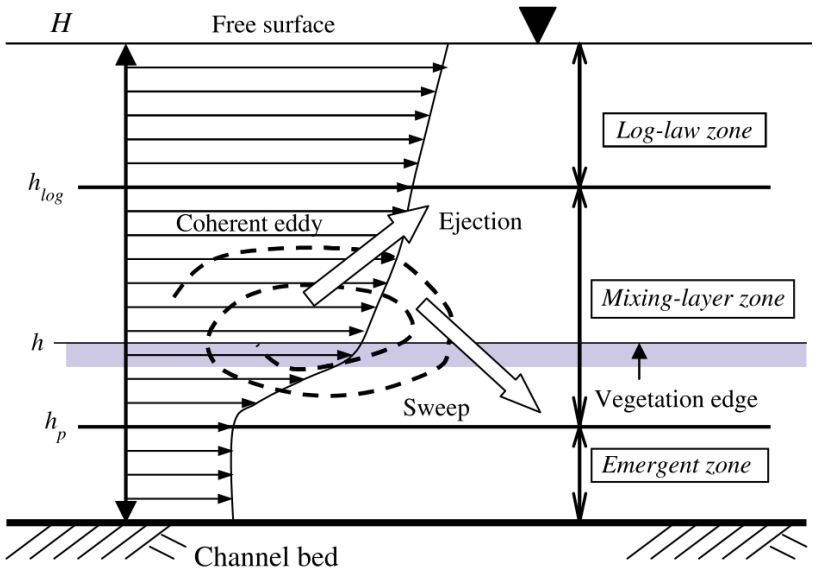

Figure 4. Flow model for aquatic vegetation flow (Nezu and Sanjou, 2008).

Most recently, Yilmazer et al. (2018) studied the effect of submergence ratio and solid volume fraction (SVF) of a vegetation patch on the velocity profiles. Their study showed that the vegetation decreases the velocity of flow both inside the vegetation layer and in the wake region. Furthermore, their experimental data revealed that vegetation with different heights has different effects on velocity profiles, for example, low SVF has small effect on the velocity profile over the vegetation layer while higher SVF causes a decline in the velocity profile along the cross-section of the channel. For the higher vegetation height, the vegetation layer affects the velocity distribution both within and over the vegetation layer. The vertical

distribution of mean velocity implied that jet flow occurs in the non-vegetated half of the channel (Yilmazer et al. 2018).

Huai et al. (2014) proposed an analytical model to predict the velocity profile using their experimental datasets. Their model may work for a different range of data; however, their model depends on a variety of coefficients and different parameters, which need to be defined and calibrated, individually.

Model Development

Based on Schlichting & Gersten (2017), and according to Boussinesq hypothesis, the turbulent shear stress can be defined as:

$$\tau(z) = \rho v_t \frac{\partial u}{\partial z} = \rho \lambda u \frac{\partial u}{\partial z} . \quad (38)$$

where v_t and λ are the total eddy viscosity of vegetated flow and the mixing length of eddy, respectively. In Eq. (38), the application of $v_t = \lambda u$ is attributed to Kolmogorov's energy cascade analysis of $v_t = c^{1/4} l \sqrt{E_t}$ where l is the length scale of eddy, c is the Kolmogorov constant and E_t is the turbulent kinetic energy. In analogous fashion, the velocity scale, u, may be taken as the square root of E_t since the turbulent fluctuations characterize the transport of momentum (Katopodes, 2019, pp 625-626), as similar to Eq. (19) by Baptist et al. (2007).

For given vegetation density of a and drag coefficient of C_D, an analytical solution can be obtained for u^2 in Eq. (20) as:

$$u^2 = \frac{2gS_0}{aC_D} + Ae^{\mu z} + Be^{-\mu z}, \quad (39)$$

where $\mu = \sqrt{\frac{a\ C_D}{\lambda}}$. The integration constant A and B can be calculated by applying the boundary conditions (Klopstra et al., 1996; Defina & Bixio, 2005; Baptist et al. 2007; Tang 2019c).

In layer 1 (see Fig. 2), at the bed where $z=0$, the bed shear stress can be neglected in comparison to the drag coefficient of vegetation. Under this assumption, the local equilibrium between gravity force and drag force of vegetation will lead to:

$$u_0 = u|_{z=0} = \sqrt{\frac{2gS_0}{aC_D}}, \quad (40)$$

At the top of the vegetation where $z=h$, the boundary shear stress is defined by:

$$\tau|_{z=h} = \rho g(H-h)S_0, \quad (41)$$

Thus, similar to the analysis of the model of Klopstra et al. (1997), the constant in Eq. (39) will become $A=-B$, hence given by:

$$A = \frac{gS_0(H-h)}{\lambda\ \mu \cosh(\mu h)}, \quad (42)$$

By inserting Eq. (42) into Eq. (39), the velocity for the first layer becomes:

$$u_{(1)} = \sqrt{u_0^2 + 2\ A \sinh(\mu_1 z)}, \quad (43)$$

where the subscript (1) denotes the region of layer 1 and u_0 is described by:

$$u_0 = \sqrt{\frac{2\ g\ S_0}{a_1\ C_D}}, \quad (44)$$

where a_1 is the parameter related to the density of vegetation and defined by:

$$a_1 = \frac{d}{\Delta s_x\ \Delta s_y}, \quad (45)$$

where d is the diameter of dowels (i.e. models of vegetation); Δs_x and Δs_y are the streamwise and lateral spacing of dowels, respectively.

Furthermore, μ_1 in Eq. (43) is defined by:

$$\mu_1 = \sqrt{\frac{a_1 C_D}{\lambda_1}}, \tag{46}$$

where λ_1 is the parameter related to the characteristic length of eddy in the flow. This parameter λ_1 is dependent on the height of vegetation and the flow depth, as suggested by Klopstra et al. (1996), Defina & Bixio (2005), Baptist et al. (2007) and Tang (2019c).

In addition, it should be mentioned that the characteristic length of eddy is associated with the coherent eddy described by Nezu and Sanjou (2008), as illustrated in Fig. 4. The mixing-layer zone is due to the substantial wake effect of vegetation in the emergent zone. Poggi et al. (2004) described the flow structure over the submerged vegetation in three zones, as shown in Fig. 5.

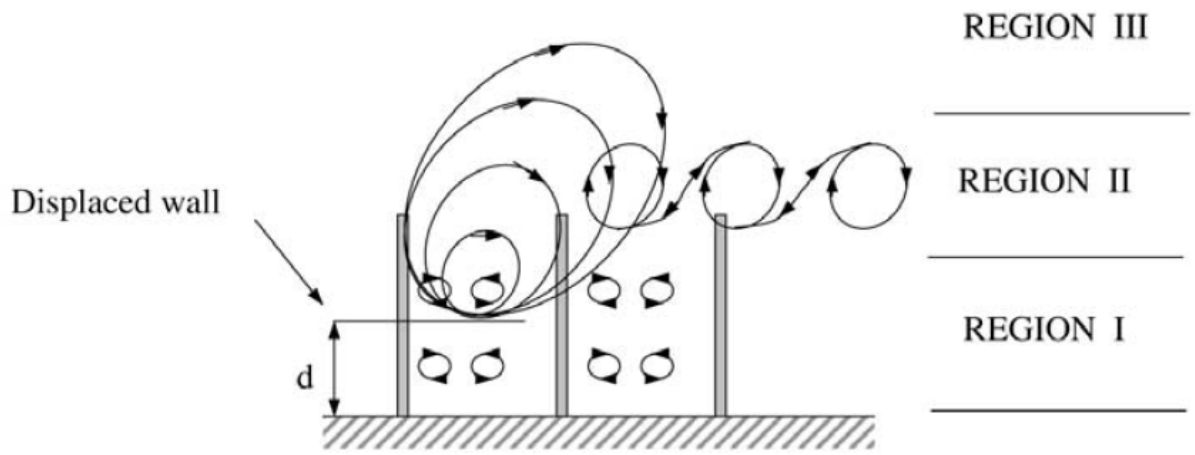

Figure 5. Sketched flow structure (Poggi et al. 2004)

This mixing length can be empirically evaluated by:

$$\lambda_1 = k_1\sqrt{(H - h_s)h_s}, \tag{47}$$

where h_s represents the short vegetation height, k_1 is a constant, whose value should be empirically evaluated, as discussed in Tang (2019c). The optimal value of k_1 was found as 0.001 in this study.

Eq. (39) still applies for the layer 2, where only tall vegetation exists (see Fig. 2), in different boundary condition. Based on the boundary condition at the free surface, where the turbulent shear stress is negligible compared with the drag force of vegetation, the velocity can then be described by a hyperbolic function profile as:

$$u_{(2)} = \sqrt{u_T^2 + C[e^{\mu_2 z} - e^{\mu_2 (2H - z)}]}, \quad (48)$$

where the subscript (2) denotes the region of layer 2, and:

$$u_T = \sqrt{\frac{2\, g\, S_0}{a_2}}, \quad (49)$$

$$\mu_2 = \sqrt{\frac{a_2\, C_D}{\lambda_1}}. \quad (50)$$

Following the continuous boundary conditions of velocity and its gradient at $z=h_s$, the constants A and C can be obtained as:

$$A = \frac{u_T^2 - u_0^2}{2\sinh(\mu_1 h_s) + 2\left(\frac{\mu_1}{\mu_2}\right)\cosh(\mu_1 h_s) tanh[\mu_2 (2H - h_s)]}, \quad (51)$$

$$C = \frac{\mu_1 cosh(\mu_1 h_s)}{\mu_2 e^{\mu_2 H} cosh[\mu_2 (H - h_s)]}. \quad (52)$$

Thus in the two-layered vegetation, where the short vegetation is fully submerged and the tall one is emergent, the two new Eqs. (43) and (48) predict the velocity profiles for layers 1 and 2, respectively.

Experiments

To test the proposed analytical model, several experiments were conducted in an open channel with two layers of vegetation where the short vegetation was fully submerged and the tall one was emergent. All the experiments were carried out in a 12m long rectangular flume of 0.4 m (width) x 0.4 m (height) at Nanjing Hydraulic Research Institute, China (Fig. 6a). The bed slope of the channel was 0.004. To obtain a uniform flow under different flow conditions and vegetation configurations, a flow straightener of different mesh sizes was used

at the entrance in the stilling tank, combined with the manual tailgate at the end of the flume. The schematic plan and vertical view of the channel are shown in Fig. 6.

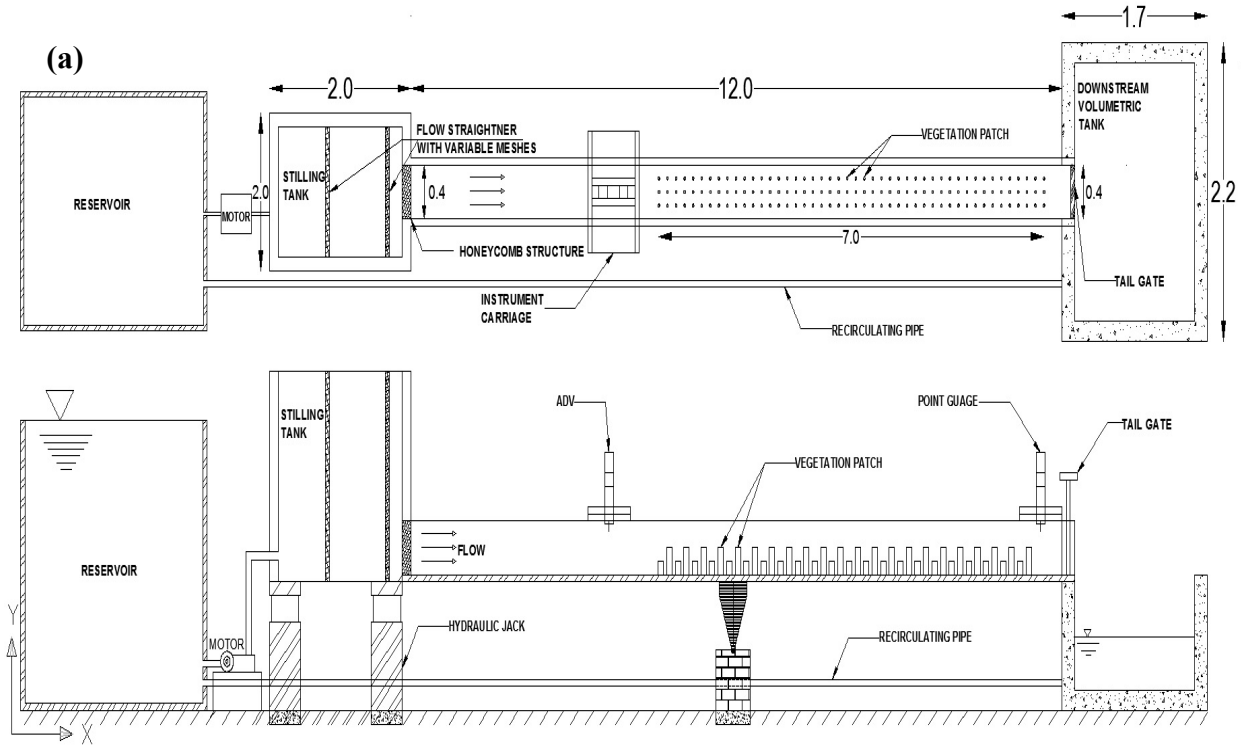

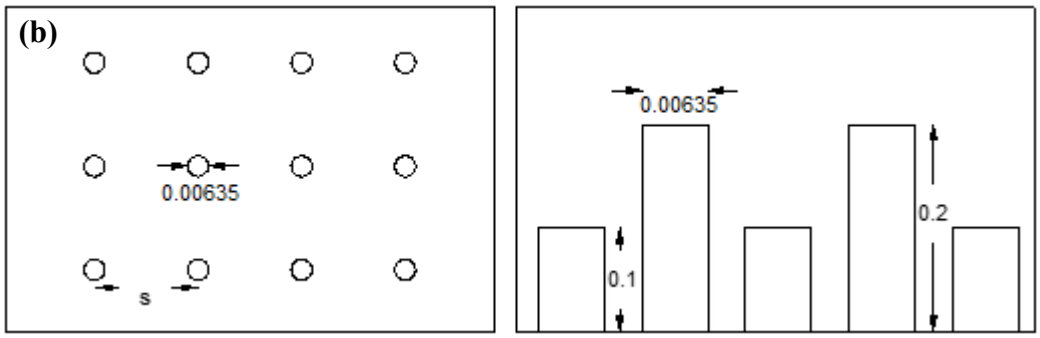

Figure 6. (a) Schematic diagram of the flume showing planar and elevation of the channel with the vegetation patch placed at 4 m downstream of the stilling tank, (b) short and tall dowels imitating two-layered vegetation with 's' being the distance between dowel (variable) and diameter as 0.00635 m (fixed).

The vegetation is modelled by circular plastic cylinders of 6.35 mm diameter with two different heights of 0.1 m and 0.2 m, which represent the short and tall vegetation, respectively (Fig. 6b). All the rigid dowels were mounted in 10 mm thick pre-perforated plates at the bottom of the flume, which covered 7 m of the channel length starting at 4 m downstream of the stilling tank.

Different measurement locations were selected to evaluate the flow characteristics in different regions of the vegetation as illustrated in Fig. 7. All the instantaneous velocity measurements (u, v, w in x, y, z direction, respectively) were taken using Nortek Acoustic Doppler Velocimetry (ADV), with an accuracy of $\pm 0.5\%$ of measured value with $\pm 1\, mm/s$. The collected datasets were processed on WinADV software. The streamwise, lateral and vertical directions are denoted by the x, y and z direction respectively, where the datum is at $z = 0$. The time-averaged velocity components and fluctuating velocities in each direction are denoted as U, V, W and u', v', w', corresponding to x, y and z direction. Based on acoustic frequency of the instrument used, the sampling volume and sampling rate of the ADV were 0.09 cm^3 and 0.1 to 50 Hz, respectively. Generally, 25 Hz is the most appropriate value since it provides the highest temporal resolution. The number of velocity measurement points varies with the distribution of signal to noise ratio (SNR) over the measurement locations.

Vegetation formation

The experiments were conducted based on combination of linear and staggered patterns for both short and tall dowels (Fig.7). The vegetation configuration was designed to resemble the vegetation in natural rivers that is usually denser in the lower layer and sparser in the upper layer (Nepf et al., 2007).

The measurement locations in Fig. 7 are denoted by small circles. These locations are tactically selected to cover the regions behind the short and tall dowels and free open region, so that velocity variation can be identified and modelled in all possible regions.

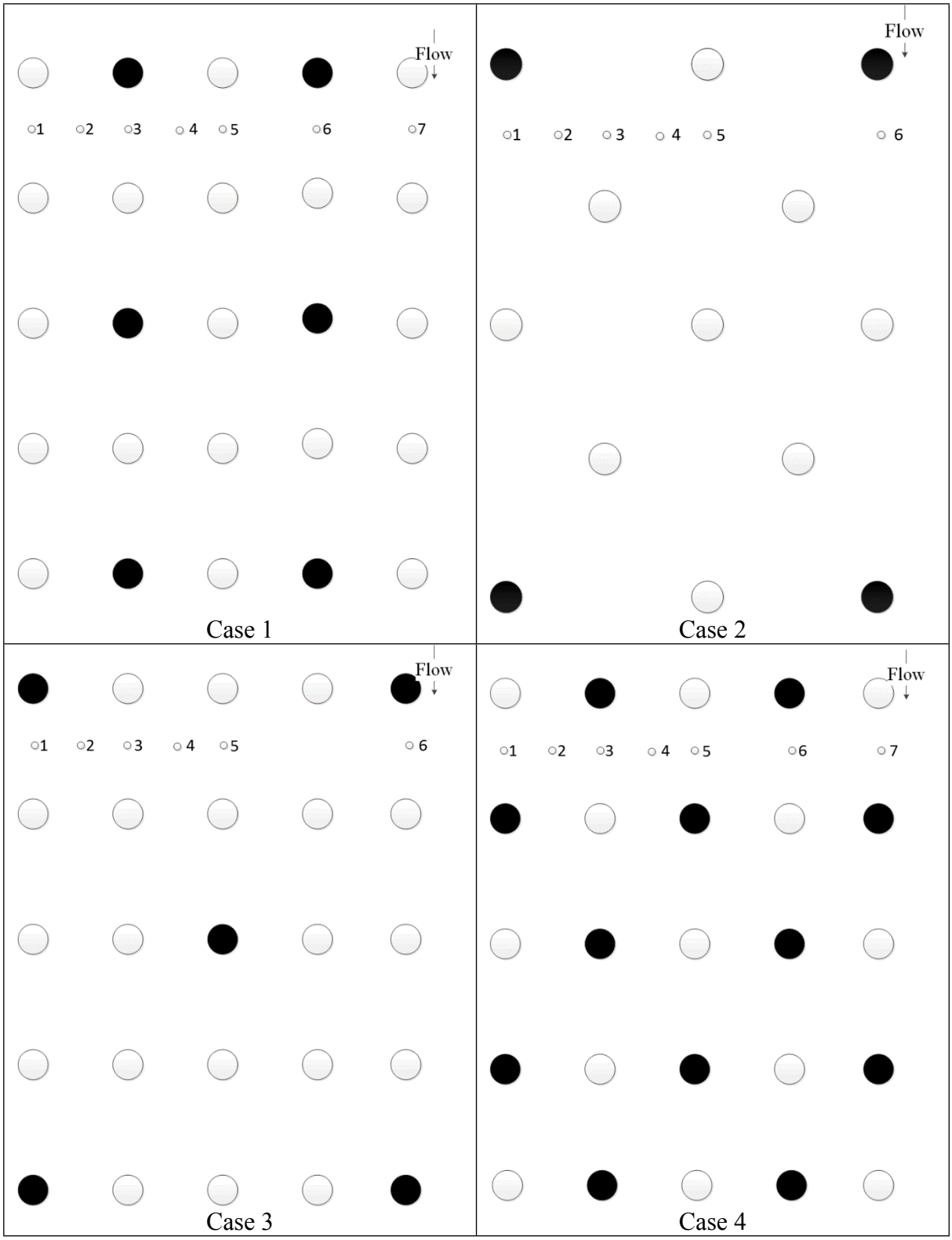

Figure 7. Dowel arrangement for Cases 1-4. The large black and white circles represent tall and short dowels, respectively. The small circles represent the measurement points by ADV.

Table 1 summarizes variables of each experiment run and its parameters used for the subsequent model test. For consistency, a uniform flow depth, with almost similar discharges

was maintained to compare the effect of different formations and spacing of vegetation in the same experimental condition.

To ensure that the proposed model is not limited to our experiments, other studies have been included (see Table 1). These data include Liu et al. (2008) and Huai et al. (2014) study which have varieties of formations of vegetation. It should be mentioned that, in all these experiments, the flow depth is somewhere between the short and tall vegetation heights. In other words, the short vegetation is fully submerged while the tall one is emergent.

In the subsequent result section, the experimental and analytical results of vertical distribution of mean streamwise velocity are presented, followed by the comparison between the proposed model and the data from Liu et al. (2010) and Huai et al. (2014).

400 **Table 1.** The flow variables and the respective datasets used for the development of the proposed model.

Author	Run	d (m)	S_x (m)	S_y (m)	H (m)	h_s (m)	h_t (m)	H/h_s	H/h_t	a_1 (m^{-1})	a_2 (m^{-1})	C_D	S_0
This study	1.1	0.00635	0.0635	0.0635	0.123	0.1	0.2	1.23	0.61	0.55	0.27	1.1	0.004
	1.2	0.00635	0.0635	0.0635	0.154	0.1	0.2	1.54	0.77	0.55	0.27	1.1	0.004
	1.3	0.00635	0.0635	0.0635	0.181	0.1	0.2	1.81	0.90	0.55	0.27	1.1	0.004
	2.1	0.00635	0.127	0.127	0.124	0.1	0.2	1.24	0.62	0.47	0.29	1.1	0.004
	2.2	0.00635	0.127	0.127	0.151	0.1	0.2	1.51	0.75	0.47	0.29	1.1	0.004
	2.3	0.00635	0.127	0.127	0.181	0.1	0.2	1.81	0.90	0.47	0.29	1.1	0.004
	3.1	0.00635	0.127	0.0635	0.123	0.1	0.2	1.23	0.61	0.55	0.27	1.1	0.004
	3.2	0.00635	0.127	0.0635	0.152	0.1	0.2	1.52	0.76	0.55	0.27	1.1	0.004
	3.3	0.00635	0.127	0.0635	0.183	0.1	0.2	1.83	0.91	0.55	0.27	1.1	0.004
	4.1	0.00635	0.0635	0.03175	0.126	0.1	0.2	1.26	0.63	0.55	0.27	1.1	0.004
	4.2	0.00635	0.0635	0.03175	0.156	0.1	0.2	1.56	0.78	0.55	0.27	1.1	0.004

	4.3	0.00635	0.0635	0.03175	0.184	0.1	0.2	1.84	0.92	0.55	0.27	1.1	0.004
Liu et al. (2010)	1	0.00635	0.0635	0.0635	0.1266	0.076	0.152	1.66	0.83	1.57	0.62	1.1	0.003
	2	0.00635	0.0635	0.0635	0.1212	0.051	0.152	2.37	0.79	1.57	0.62	1.1	0.003
	4	0.00635	0.0508	0.0508	0.1027	0.076	0.152	1.35	0.67	1.22	0.30	1.1	0.003
	5	0.00635	0.0508	0.0508	0.1046	0.076	0.152	1.37	0.68	0.83	0.30	1.1	0.003
	6	0.00635	0.1016	0.1016	0.0922	0.076	0.152	1.21	0.60	0.55	0.48	1.1	0.003
	7	0.00635	0.1016	0.1016	0.094	0.076	0.152	1.23	0.61	0.61	0.24	1.1	0.003
Huai et al. (2014)	X1	0.006	0.11	0.053	0.207	0.14	0.24	1.47	0.86	1.02	0.51	1.13	0.00034
	X2	0.006	0.11	0.053	0.233	0.14	0.24	1.66	0.97	1.02	0.51	1.13	0.00034
	Y1	0.006	0.11	0.053	0.207	0.14	0.24	1.47	0.86	1.02	0.51	1.13	0.00032
	Y2	0.006	0.11	0.053	0.233	0.14	0.24	1.66	0.97	1.02	0.51	1.13	0.00034

401 Note: S_x and S_y are the distances of the dowels in *x* and *y* directions, respectively.

402

403

Experimental Results and Discussion

Comparisons between measured and modelled longitudinal velocity profiles are shown in Fig. 9. The velocity data marked as 'ave' are the spatial average of velocity from different locations in individual cross section of each case (as marked in Fig. 7). Spatial averaging of the data here is required because the mean momentum balance already assumes a planar averaging carried out by Raupach and Shaw (1982). The averaging is calculated by weighted average method, where the weights were selected as a parameter related to the diameters of dowels and the space between centres of two adjacent dowels. For example in Fig. 8, locations in free region have the highest velocity compared to those behind the dowels (Liu et al., 2008; Rahimi et al., 2019), either short or tall, so they have the highest coefficient that is $s-d$, otherwise, the locations behind the dowels have the coefficient of $d/2$.

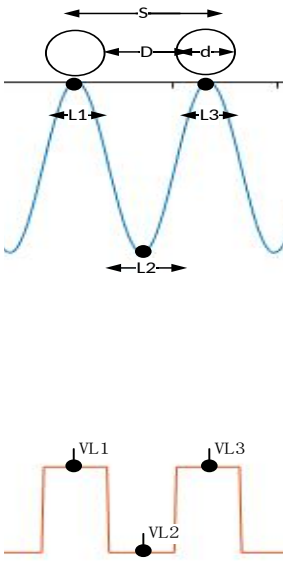

Figure 8. Weighted average method for Cases 1-4 (plan view). The big white circles represent dowels while the small bold circles represent the measurement points by ADV.

Therefore , the weighted average velocity (V_{ave}) is calculated by:

$$V_{\text{ave}} = \frac{\frac{V_{L1}d}{2} + V_{L2}(s-d) + \frac{V_{L3}d}{2}}{d+D}, \quad (53)$$

where V is the velocity at different locations, d is the diameter of each dowel, D is the distance between two adjacent dowels, and s is the distance between the centres of two adjacent dowels.

Fig. 9 summarizes all the runs of our experiments for completeness. Among all the runs the largest velocity occurs in the free regions, such as L2 and L4. The least velocity is found in the regions downstream of the dowels (locations L1, L3, L5, L6, and L7) irrespective of the dowel height in the uniform velocity zone ($z < h_s$). Locations L3 and L6 are behind the tall dowels with the velocity profile also having least velocity throughout the sections. These observations from L3 and L6 show that the fluid experiences most drag in these regions. Inflection spike in these profiles is not significant, which is not the same as the case with the profiles at locations L1, L5 and L7. In these locations where the short dowel is completely submerged, inflection over the height of $z = h_s$ is significant with a sudden increase in velocity immediately above $z = h_s$.

Similarly, in experiment 1.1, 2.1, 3.1 and 4.1 (Figs. 9a, d, g & j respectively) the minimum depth of flow was maintained at 12 cm, the velocity appears a similar trend to that of flow with single layer vegetation. The velocities in these runs are found to be almost constant throughout the height of short vegetation, followed by a rapid increase in velocity at $z = h_s$. However, the spatial variation (L1-L6 or L7) of velocity trend is observed in each case from linear-linear to staggered-staggered formation (see Fig. 9). For the other runs, i.e. experiments 1.2, 1.3, 2.2, 2.3, 3.2, 3.3, 4.2 and 4.3 (Fig. 9b, c, e, f, h, i, k and l), velocity increases rapidly near the top of the

441 short vegetation $h_s = 0.1m$, and the increase in velocity becomes larger with increasing depth in
442 all the cases. Furthermore, in the sparser dowel arrangements with high flow depth (experiment
443 2.3), multiple inflections in velocity profile can be seen in locations L1, L2, L4 and L5. The
444 increment in the velocity above zero plane displacement is also found to be dependent on the
445 location proximity to the tall dowels. About 15-18% is found for the variation in velocity above
446 $z = h_s$at location L5 (behind short dowel in the mid-section of the configuration) in experiments
447 1.1, 1.2 and 1.3 (Figs. 9a, b, and c). On the other hand, with sparser arrangement at location L5
448 the percentage increment in velocity above $z = h_s$ is found to be around 9-13% in experiments
449 2.1-2.3 (see Figs. 9 d-f).

450 In Figs. 9g-9l with sparser arrangement of tall dowels, the velocity profile does not become
451 constant immediately behind locations L3 and L6, while in other locations the velocity is least.
452 Moreover, the velocity above $z > h_s$ does not appear to converge onto a single logarithmic
453 profile after slip velocity. This could be attributed to the effect from the depth of submergence of
454 the tall dowel. In these cases, drag dominates throughout the column of flow behind tall dowels.
455 However, in case of complete submergence both turbulent stress and wake effects come into
456 action in the region close to the surface, in which a logarithmic velocity applies.

457

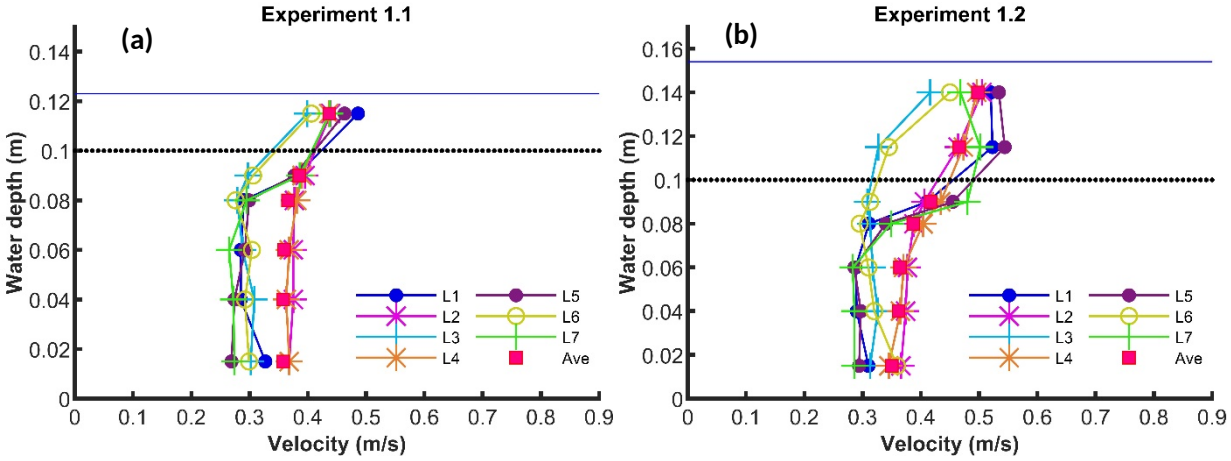
Experiment 1.1
(a)
Experiment 1.2
(b)
Water depth (m)
Velocity (m/s)
L1
L2
L3
L4
L5
L6
L7
Ave

458

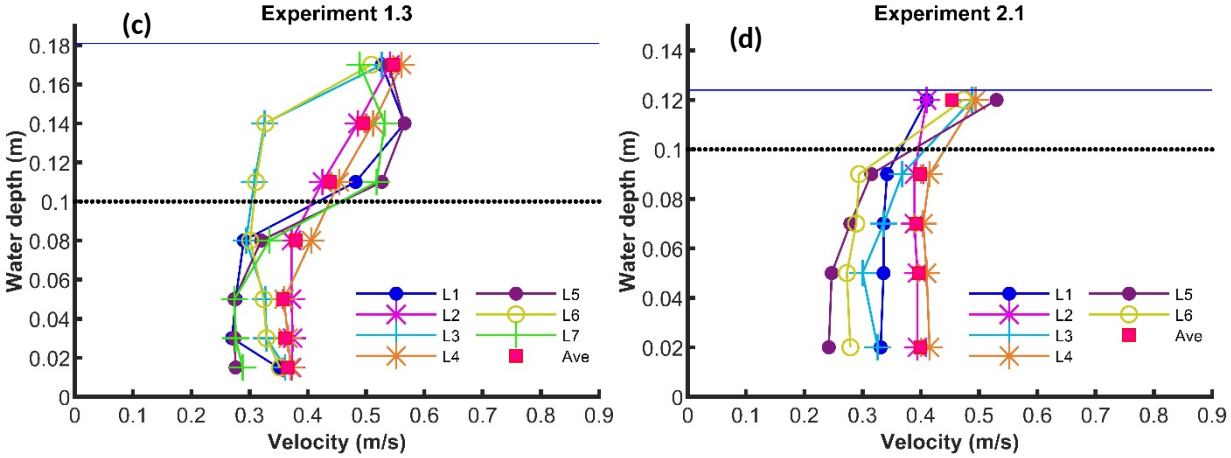
Experiment 1.3
(c)
Experiment 2.1
(d)
Water depth (m)
Velocity (m/s)
L1
L2
L3
L4
L5
L6
L7
Ave

459

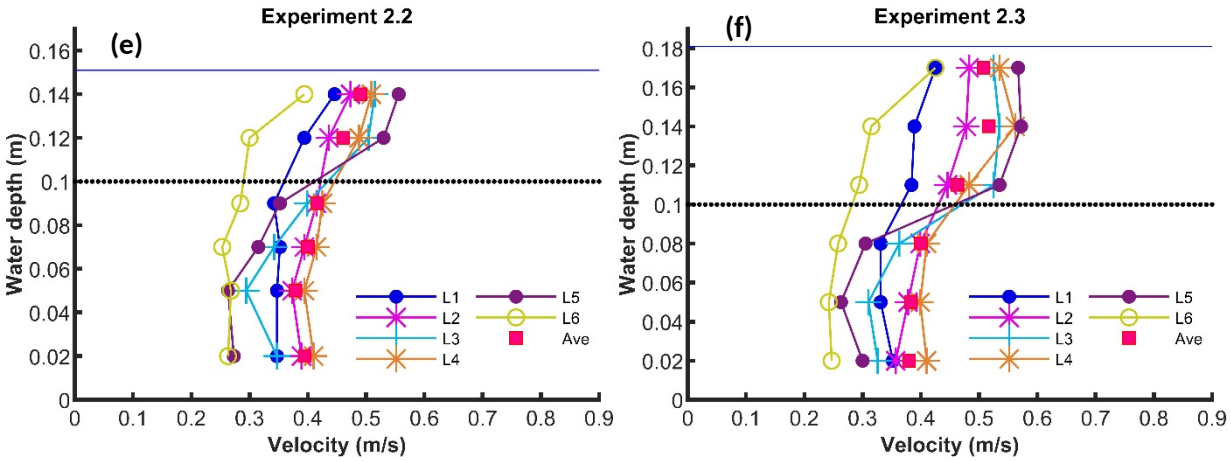
Experiment 2.2
(e)
Experiment 2.3
(f)
Water depth (m)
Velocity (m/s)
L1
L2
L3
L4
L5
L6
Ave

460

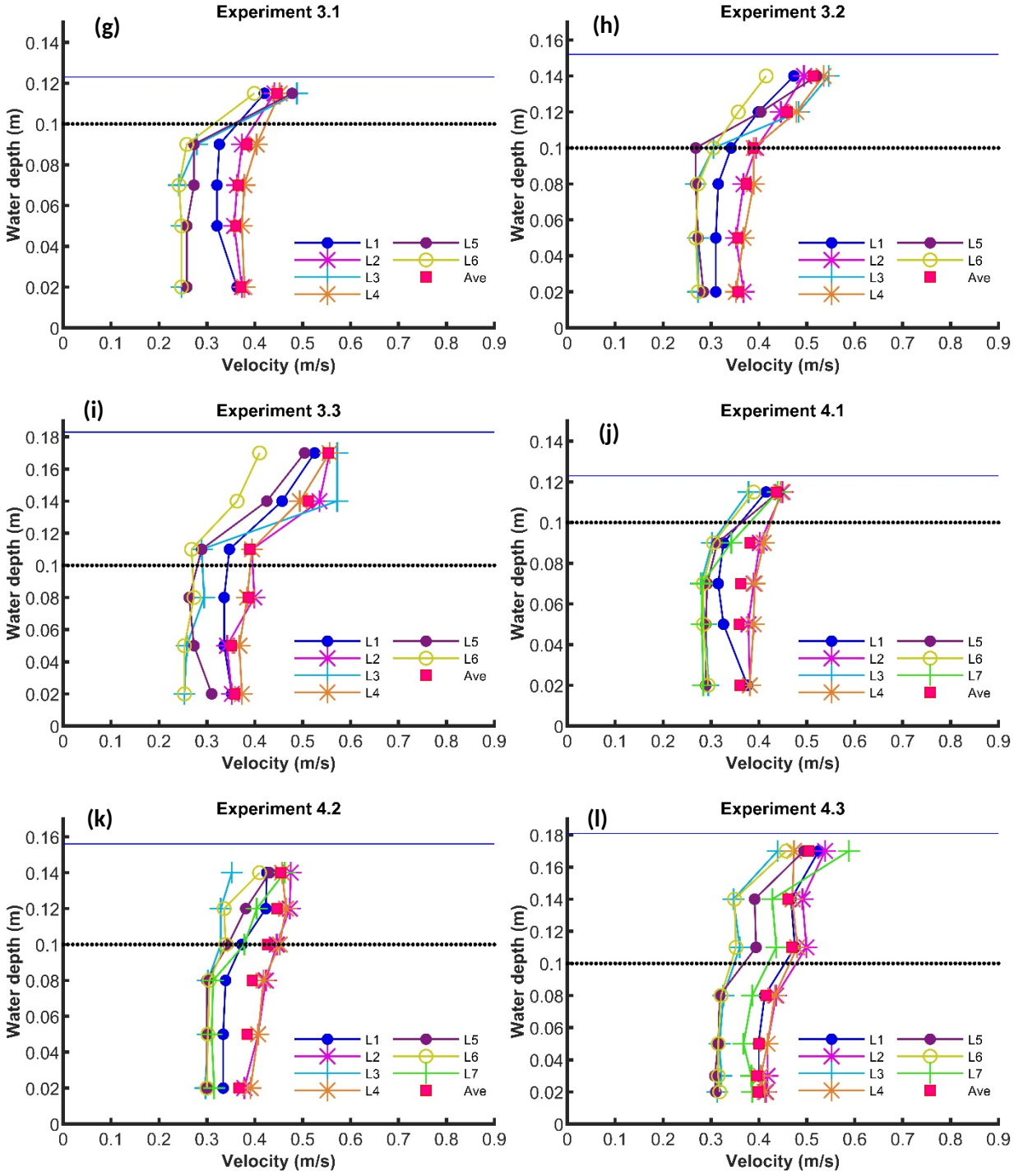

461

462

463

464 **Figure 9.** Experimental data for four different formations under three different flow depths: **(a), (b) & (c)** for short
465 and tall dowels located in a linear formation (Case 1) under the flow depths of 0.123, 0.154 & 0.181 m respectively;
466 **(d), (e) & (f)** for short and tall dowels located in staggered and linear formations with sparser arrangements (Case 2)
467 under the flow depths of 0.124, 0.151 & 0.181 m respectively; **(g), (h) & (i)** for short and tall dowels located in
468 linear and staggered formations (Case 3) under the flow depths of 0.123, 0.152 & 0.183 m respectively; **(j), (k) & (l)**
469 for both short and tall dowels located in staggered formations (Case 4) under the flow depths of 0.126, 0.156 &
470 0.184 m respectively. The dotted line denotes the top of the short vegetation and the blue solid line represents the
471 water surface.

Model Application

To test the analytical model on data sets not used in its calibration, the following published experiments are used: Fig. 11 for experiments by Liu et al. (2010) and Fig. 13 for experiments in Huai et al. (2014). A total of 22 runs were considered without any biased selection (see Table 1), with vegetation height varying from $0.051 \leq h_s \leq 0.14$ and $0.152 \leq h_t \leq 0.24$, flow depth from $0.12 \leq H \leq 0.23$, the frontal area of vegetation from $0.47 \leq a_1 \leq 1.57$ and $0.27 \leq a_2 \leq 0.62$, and drag coefficient from $1.1 \leq c_D \leq 1.13$.

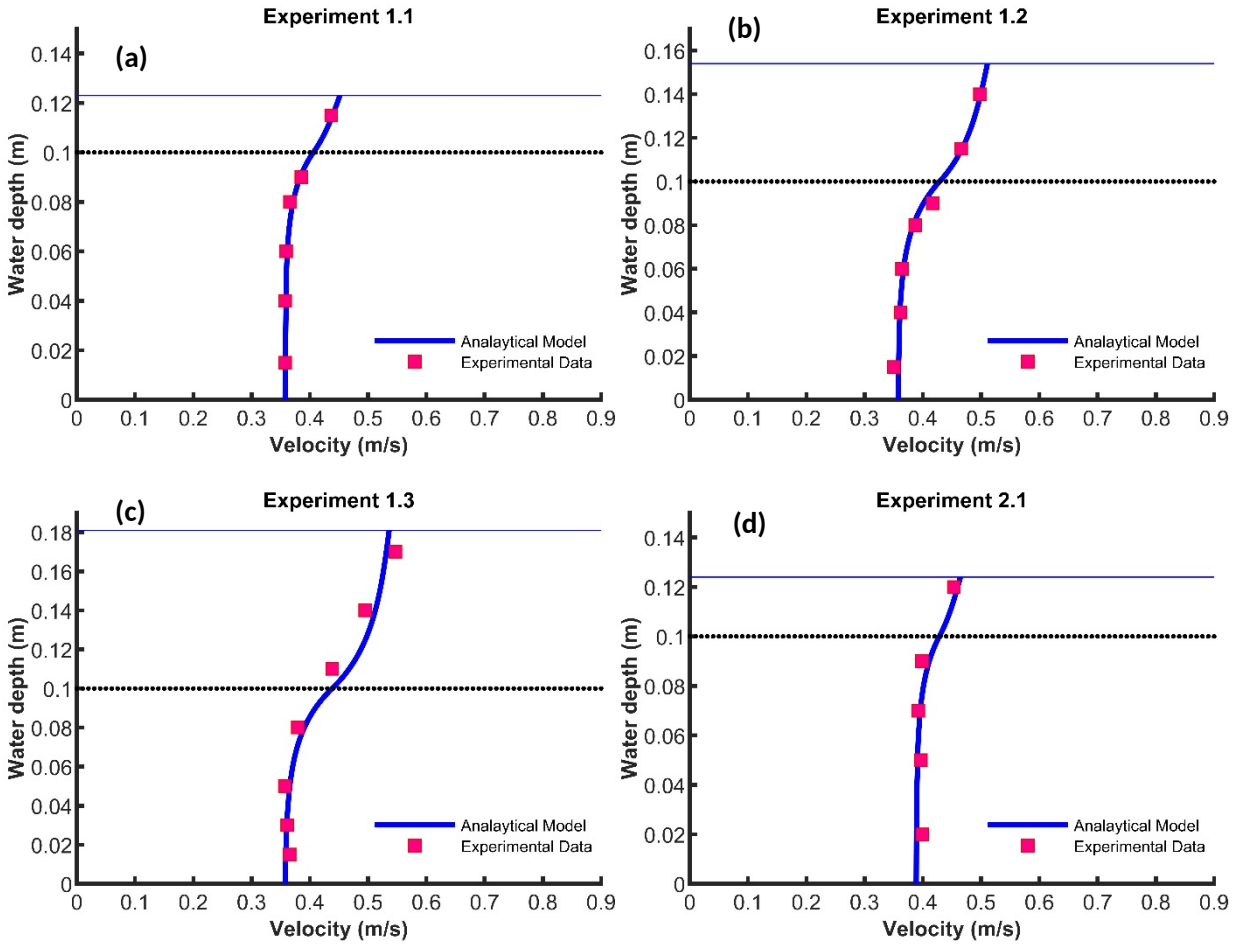

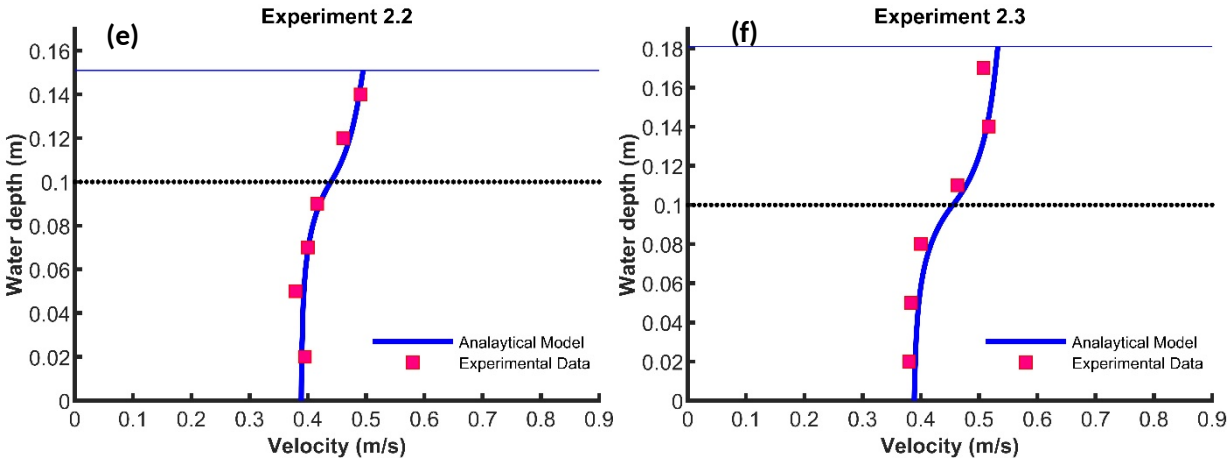
(e)
Experiment 2.2
(f)
Experiment 2.3
Water depth (m)
Velocity (m/s)
Analaytical Model
Experimental Data

483

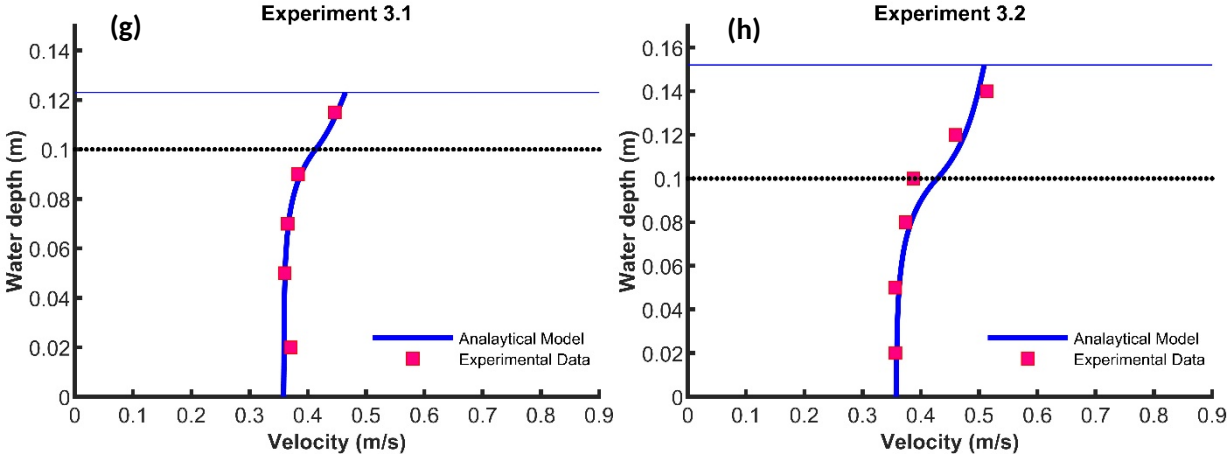
(g)
Experiment 3.1
(h)
Experiment 3.2
Water depth (m)
Velocity (m/s)
Analaytical Model
Experimental Data

484

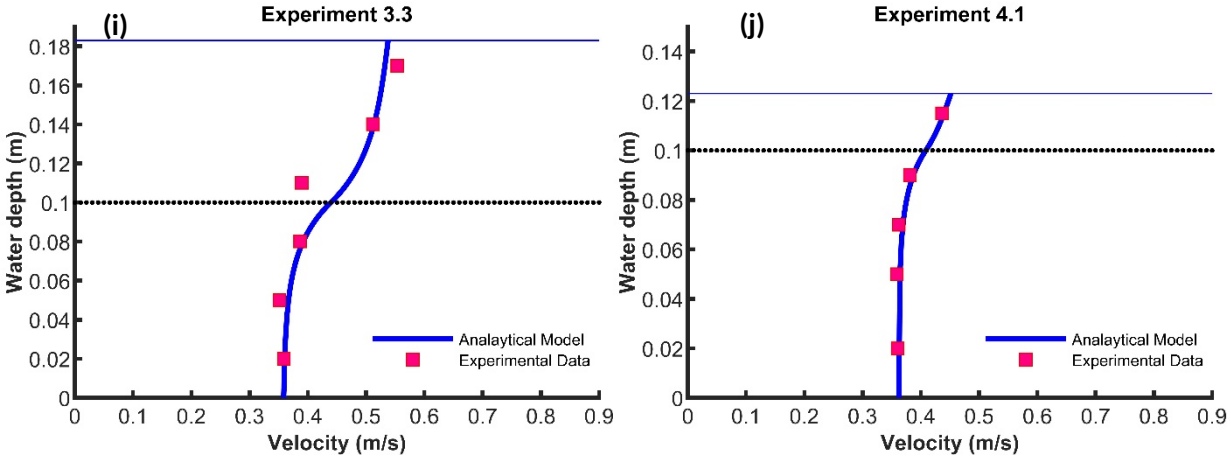
(i)
Experiment 3.3
(j)
Experiment 4.1
Water depth (m)
Velocity (m/s)
Analaytical Model
Experimental Data

485

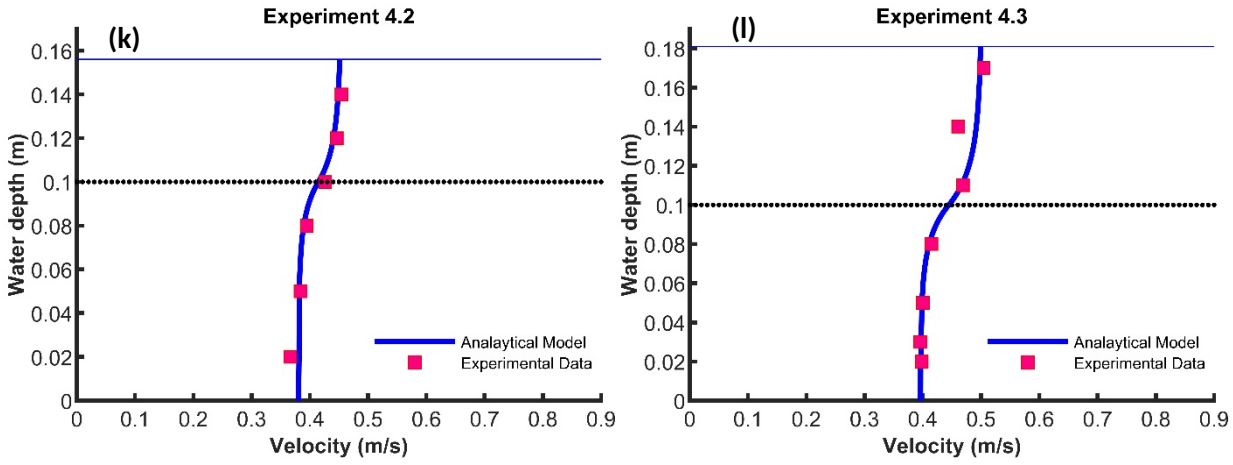

Figure 10. Comparison of the proposed analytical model with our experimental data. The dotted line denotes the top of the short vegetation and the blue solid line represents the water surface.

The averaged velocity of weighted experimental data and analytical results are compared in Fig.10. This shows an overall good agreement between the experimental and predicted velocities. In experiments 1.1, 1.2, and 1.3 with linear formations for both short and tall dowels (Case 1), the analytical model shows good agreement with experimental data. However, there is a slight difference at the edge of short and tall vegetation for experiment 1.3 where the flow depth of 18.1 cm is very close to the height of tall vegetation. This difference in the figure demonstrates the complexity in the flow near the edge of dowels. In experiments 2.1, 2.2 and 2.3 where the short and tall vegetation are in staggered and linear formations respectively (Case 2), there is also good agreement between analytical and experimental data with high correlations. Moreover, in experiments 3.1, 3.2 and 3.3 the experimental and predicted data agree, except at the edge of vegetation in experiments 3.3. In the high flow depth of 18.3 cm, i.e. experiment 3.3, although both experimental and analytical data have the same trend, the agreement is not as good as that in the lower depth run, 12.3 cm in experiment 3.1. Nevertheless, the model agrees with

the experimental data with staggered formations for both short and tall vegetation, see experiments 4.1, 4.2 and 4.3 in Fig. 10.

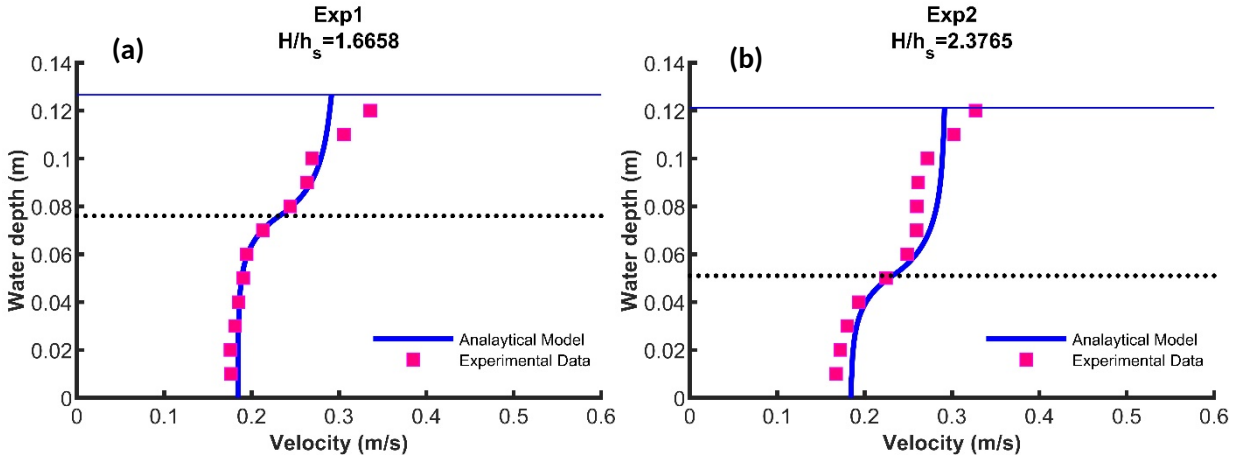

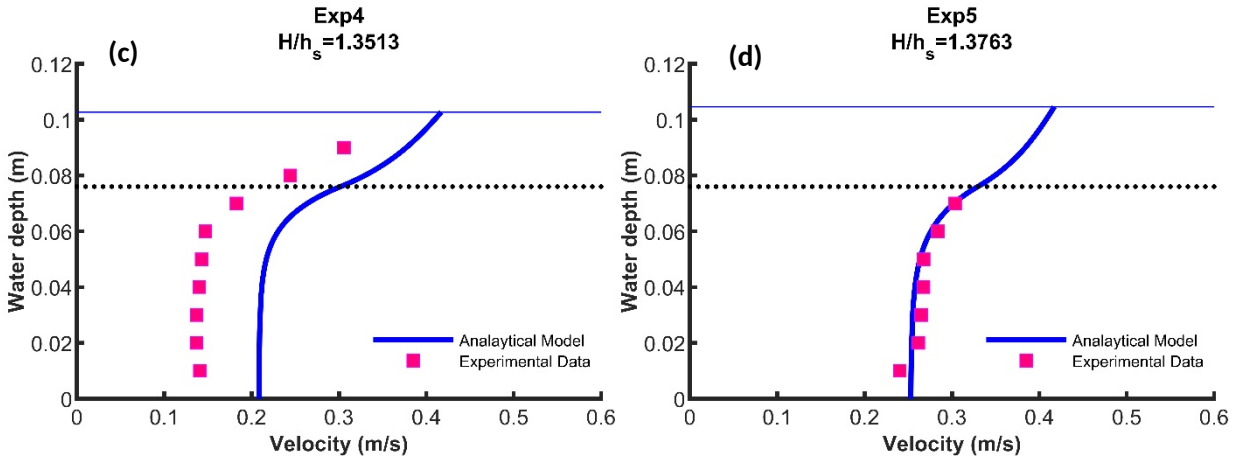

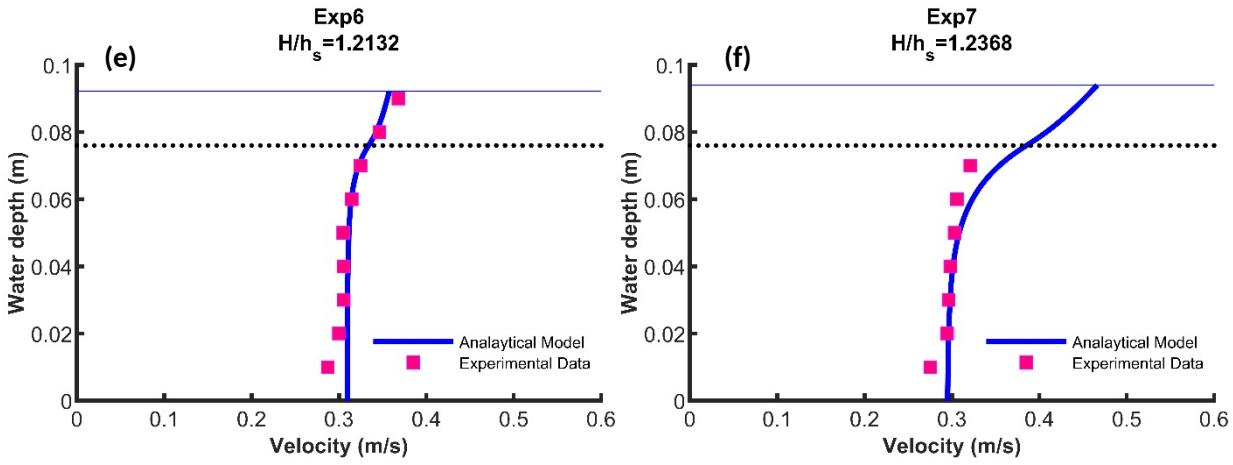

508

509 **Figure 11.** Comparison of the proposed analytical model with the experimental data of Liu et al. (2010). The dotted
510 lines is the top of the short vegetation and the blue solid line represents the water surface.
511

512 In Fig. 11, the proposed model is compared with the datasets of Liu et al. (2010), which are
513 spatially averaged. The results in Figs. 11 (a), (b) and (f) are for staggered-staggered
514 configurations with varying vegetation heights (see Table 1), whereas in Figs. 11 (c), (d) and (e)
515 short and tall vegetation is configured as the combination of linear-staggered, linear-linear and
516 staggered-linear, respectively (see Fig. 12). A sharp inflection point at $z = h_s$ is visible in all the
517 datasets, which justifies that the slip velocity lies in the region close to short vegetation height in
518 all the cases (Fig. 11). In the datasets of Liu et al. (2010), the variation of the dowel height has
519 affected the profile in the region of $z > h_s$. For instance, in Figs. 11 (a) and (d) the velocity
520 profile in the region of $z > h_s$ is not converging towards the logarithmic shape. On the other
521 hand, flow is able to achieve a constant velocity, which shows the great influence of the
522 submergence ratio of the short dowel and independent behaviour of the tall dowel, see Fig. 11
523 (c), (d), (e) and (f).

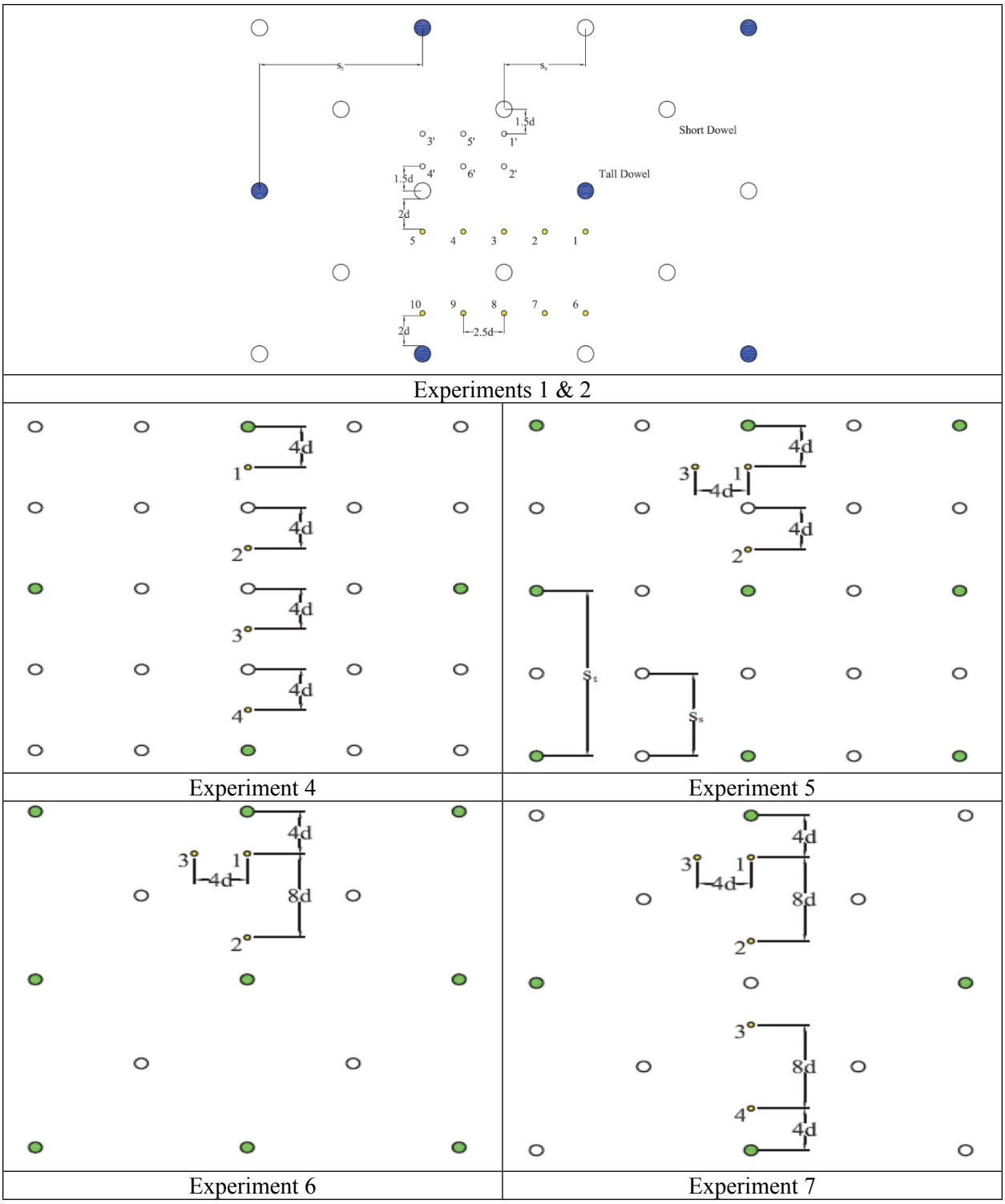

Figure 12. Formation of dowels in Liu at al. (2010) experimental data. The dowels are shown as large circles, with the solid and blank circles representing the tall and short dowels respectively. The small circles denote the measurement locations.

In experiment 4 of Liu et al. (2014), all the measurement locations are behind the dowels and there is no measurement in the free region area (see Fig. 12). The lack of measurement in the free region affects the spatially weighted average, consequently resulting in a smaller spatial average velocity, so the average velocity in Fig. 11 (c) is less than the trend of analytical model prediction. Therefore, it is not surprising that analytical and experimental data did not show good agreement in experiment 4.

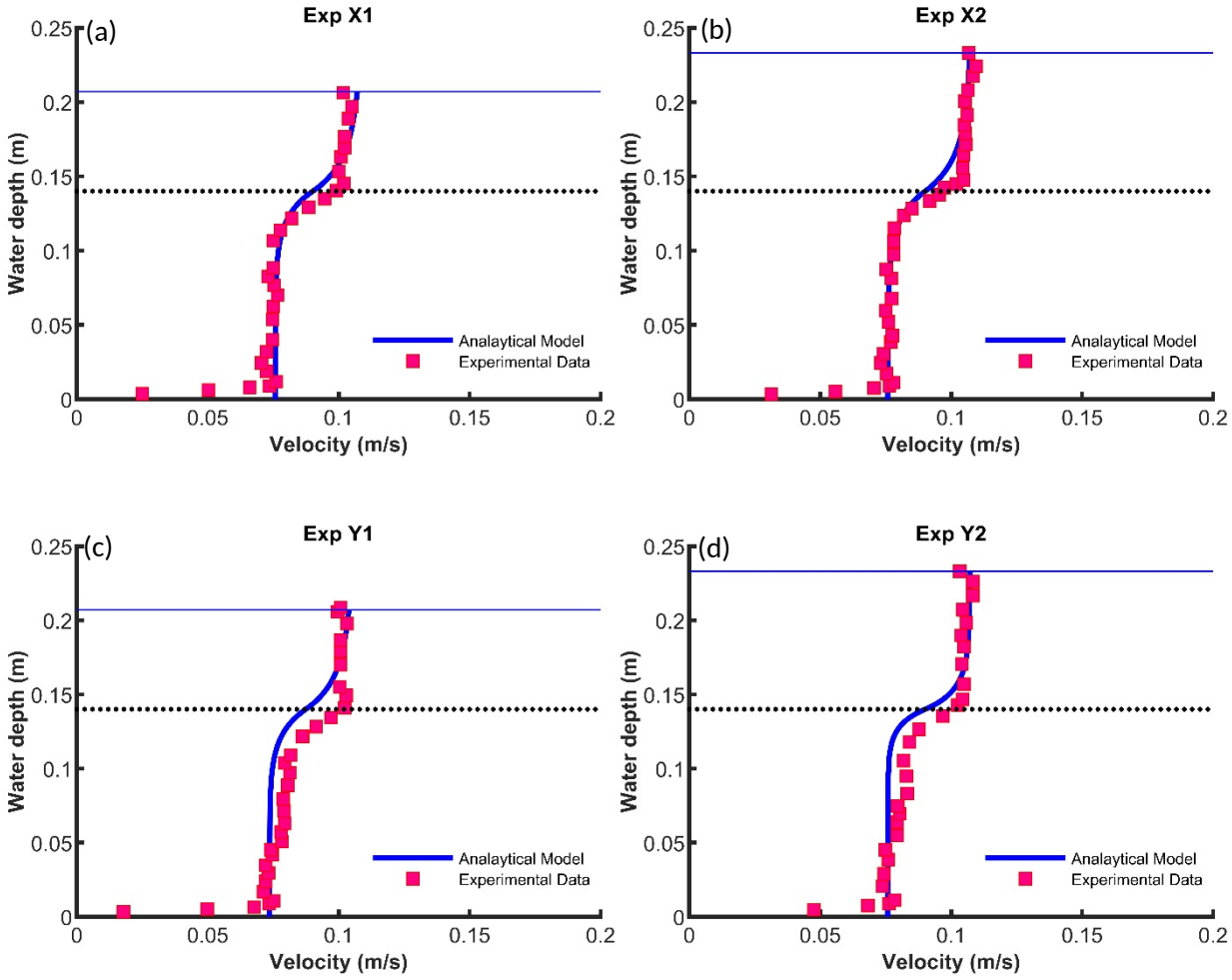

Figure 13. Comparison of the proposed analytical model with the experimental data of Huai et al. (2014). The dotted lines is the top of the short vegetation and the blue solid line represents the water surface.

The experimental datasets of Huai et al. (2014) are spatial average of the complete frame of the PIV data for their experiments X1, X2, Y1 and Y2, where X1 and X2 are linear-linear

configurations but Y1 and Y2 are staggered-staggered configurations with two flow depths (see Table 1). The velocity data as the function of z have been taken with the spatial average over 22 cm width of the camera field in the streamwise direction, which is finally averaged transversely across the test section (Huai et al., 2014). Fig. 13 shows the comparison between the data of Huai et al. and the analytical model. In general, the proposed model shows reasonably good agreement.

Discussion

To further check the robustness of the proposed model with the experiments, error analyses are carried out. The values of RMSE (Root Mean Square of Errors) have been given for different cases of vegetation formations and flow depths in Table 2.

RMSE is given by:

$$RMSE = \sqrt{\frac{1}{n}\sum_{i=1}^{n}(u_a^n - u_e^n)^2}, \quad (54)$$

where u_a is the predicted velocity by the analytical model, u_e is the measured velocity data from experiments, and n is the number of data.

Table 2. RMSE of velocity in m/s for different experiments.

Cases	1.1	1.2	1.3	2.1	2.2	2.3	3.1	3.2	3.3	4.1	4.2	4.3
RMSE	0.0022	0.0069	0.0154	0.0080	0.0083	0.0095	0.0060	0.0194	0.0342	0.0020	0.0085	0.0123

The small values of RMSE in Table 2 show agreement between analytical and experimental results. In experiments 1.1, 2.1, 3.1 and 4.1, where the flow depths are around 12 cm, the analytical model performed exceptionally well, while in experiments 1.3, 2.3, 3.3 and 4.3, where the flow depths are relatively high around 18 cm, the model comparatively underestimates in the

region of $h_s \leq z \leq h_t$. One of the reasons may be due to the complexity of flow with an increase in shear over the slip velocity around $z = h_s$, which may lead to an increase in flow velocity. Moreover, the influence of short and tall vegetation heights on the mixing layer can be further speculated as another reason for slight under-performance in the region $h_s \leq z \leq h_t$.

Based on Fig. 13, although Huai et al. (2014) proposed a different analytical model for two layered vegetation with calibration using their own experimental data, the large number of parameters with various constants in their model made it complicated and difficult to apply. On the other hand, the accuracy of their model to capture the point of inflection on the edge of short vegetation appears less in this proposed model.

Conclusions

The two layered vegetation was modelled by PVC cylindrical dowels to study vegetated flow, which was found to be more complex compared with the single layered flow. The flow velocity characteristics at different locations were studied by 3D ADV that for doubly layered vegetation with different densities and formations. A new analytical model was proposed to describe the velocity profile in two-layered vegetative flow with tall vegetation being emergent. The main finding here is that the planar averaging is necessary in such-data model comparisons. Moreover, eddy-viscosity models that are based on a local mean velocity and a prescribed mixing length appear to be reasonable, at least in such class of models.

Future work

The proposed analytical model in this study can evaluate velocity profiles in the cases where the short vegetation is fully submerged but tall ones are emergent. This often occurs in nature, but in

583 some conditions, especially in extreme flood conditions, both short and tall vegetation could be
584 fully submerged. The future studies will be focusing on studying the flow with fully submerged
585 conditions for both short and tall vegetation, which include both experimental study and
586 analytical model development.

587 **Acknowledgement**

588 The authors would like to thank the staff of Nanjing Hydraulic Research Institute for their
589 support and time during the experiments and also acknowledge the support by the Research
590 Development Fund (RDF-15-01-10, RDF-16-02-02), Key Programme Special Fund (KSF-E-17)
591 of XJTLU and National Natural Science Foundation of China (11772270). The authors would
592 also like to thank two anonymous reviewers and the editor of the journal for their constructive
593 comments, which helped to improve the paper.

594

595

596

597 **References**

598 Baptist, M. J., Babovic, V., Rodríguez Uthurburu, J., Keijzer, M., Uittenbogaard, R. E., Mynett,
599 A., & Verwey, A. 2007. On inducing equations for vegetation resistance. Journal of Hydraulic
600 Research, 45(4), 435-450.
601
602 Banerjee, S., Naik, B., Singh, P., Khatua, K. K. 2018. Flow resistance in gravel bed open channel
603 flows case: intense transport condition. ISH J. Hydraul. Eng. 25:3, 298-309.
604 https ://doi.org/10.1080/09715 010.2017.14221 89
605
606 Belcher, S. E., Jerram, N., & Hunt, J. C. R. 2003. Adjustment of a turbulent boundary layer to a
607 canopy of roughness elements. Journal of Fluid Mechanics, 488, 369-398.
608
609 Carollo, F. G., Ferro, V., and Termini, D. 2002. Flow velocity measurements in vegetated
610 channels. Journal of Hydraulic Engineering, 128(7), 664-673.

611 Defina, A., & Bixio, A. C. 2005. Mean flow and turbulence in vegetated open channel flow.
612 Water resources research, 41(7).

Ghisalberti, M., and Nepf, H. 2006. The structure of the shear layer in flows over rigid and flexible canopies. Environmental Fluid Mechanics, 6(3), 277-301.

Huai, W., Wang, W., Hu, Y., Zeng, Y., and Yang, Z. 2014. Analytical model of the mean velocity distribution in an open channel with double-layered rigid vegetation. Advances in water resources, 69, 106-113.

Huthoff, F., Augustijn, D., & Hulscher, S. J. 2007. Analytical solution of the depth-averaged flow velocity in case of submerged rigid cylindrical vegetation. Water resources research, 43(6).

Ikeda, S., and Kanazawa, M. 1996. Three-dimensional organized vortices above flexible water plants. Journal of Hydraulic Engineering, 122(11), 634-640.

Katopodes, N. D. 2019. Free-surface flow – Environmental fluid mechanics. 1st edition, Butterworth-Heineman, Oxford.

Katul, G. G., Poggi, D., & Ridolfi, L. 2011. A flow resistance model for assessing the impact of vegetation on flood routing mechanics. Water Resources Research, 47(8).

Klopstra, D., Barneveld, H. J., Noortwijk, J. M., & Velzen, E. H. 1997. Analytical Model for Hydraulic Roughness of Submerged Vegetation. In Proceeding of 27th Congress of IAHR, Theme A (pp. 775-780). New-York: American Society of Civil Engineers (ASCE).

Kouwen, N., Unny, T. E., and Hill, H. M. 1969. Flow retardance in vegetated channels. Journal of the Irrigation and Drainage Division, 95(2), 329-344.

Kubrak, E., Kubrak, J., & Rowiński, P. M. 2008. Vertical velocity distributions through and above submerged, flexible vegetation. Hydrological sciences journal, 53(4), 905-920.

Liu, D., Diplas, P., Fairbanks, J. D., and Hodges, C. C. 2008. An experimental study of flow through rigid vegetation. Journal of Geophysical Research: Earth Surface, 113(F4).

Liu, D., Diplas, P., Hodges, C. C., and Fairbanks, J. D. 2010. Hydrodynamics of flow through double layer rigid vegetation. Geomorphology, 116(3-4), 286-296.

López, F., and García, M. H. 2001. Mean flow and turbulence structure of open-channel flow through non-emergent vegetation. Journal of Hydraulic Engineering, 127(5), 392-402.

Meijer, D. G., & Van Velzen, E. H. 1999. Prototype-scale flume experiments on hydraulic roughness of submerged vegetation. In 28th International IAHR Conference, Graz.

Nepf, H. M. 1999. Drag, turbulence, and diffusion in flow through emergent vegetation. Water resources research, 35(2), 479-489.

Nepf, H. M., and Vivoni, E. R. 2000. Flow structure in depth-limited, vegetated flow." Journal of Geophysical Research: Oceans, 105(C12), 28547-28557.

Nepf, H., White, B., Lightbody, A., and Ghisalberti, M. 2007. Transport in aquatic canopies. In Flow and Transport Processes with Complex Obstructions, 221-250.

Nezu, I., and Sanjou, M. 2008. Turburence structure and coherent motion in vegetated canopy open-channel flows. Journal of hydro-environment research, 2(2), 62-90.

Nikora, N., Nikora, V., & O'Donoghue, T. 2013. Velocity profiles in vegetated open-channel flows: combined effects of multiple mechanisms. Journal of Hydraulic Engineering, 139(10), 1021-1032.

Okamoto, T. A., & Nezu, I. 2013. Spatial evolution of coherent motions in finite-length vegetation patch flow. Environmental fluid mechanics, 13(5), 417-434.

Poggi, D., Porporato, A., Ridolfi, L., Albertson, J. D., & Katul, G. G. 2004. The effect of vegetation density on canopy sub-layer turbulence. Boundary-Layer Meteorology, 111(3), 565-587.

Rahimi, H. R., Tang, X., & Singh, P. 2019. Experimental and Numerical Study on Impact of Double Layer Vegetation in Open Channel Flows. Journal of Hydrologic Engineering, (ASCE) 25 (2). doi: 10.1061/(ASCE)HE.1943-5584.0001865

Raupach, M., Finnigan, J. J., & Brunet, Y. 1996. Coherent eddies and turbulence in vegetation canopies: the mixing-layer analogy. In Boundary-Layer Meteorology 25th Anniversary Volume, 1970–1995 (pp. 351-382). Springer, Dordrecht.

Raupach, M. & Shaw, R.H. 1982. Averaging procedures for flow within vegetation canopies. Boundary-Layer Meteorology, 22(1), 79-90.

Schlichting, H., & Gersten, K. 2017. Fundamentals of Boundary–Layer Theory. In Boundary-Layer Theory (pp. 29-49). Springer, Berlin, Heidelberg.

Singh, P., Rahimi, H.R., Tang, X. 2019a. Parameterization of the modeling variables in velocity analytical solutions of open-channel flows with double-layered vegetation. Environmental Fluid Mechanics, 19(3): 765-784. DOI: 10.1007/s10652-018-09656-8

Singh, P., Naik, B., Tang, X., Khatua, K. K., Kumar, A., & Banerjee, S. 2019b. Models for kinetic energy and momentum correction coefficients for non-prismatic compound channels using regression and gene expression programming. SN Applied Sciences, 1(10), 1229. Doi:10.1007/s42452-019-1222-9

Stoesser, T., Kim, S. J., & Diplas, P. 2010. Turbulent flow through idealized emergent vegetation. Journal of Hydraulic Engineering, 136(12), 1003-1017.

Stone, B. M., and Shen, H. T. 2002. Hydraulic resistance of flow in channels with cylindrical roughness. Journal of hydraulic engineering, 128(5), 500-506.

Tang, X. and Ali, S. 2013. Evaluation of methods for predicting velocity profiles in open channel flows with submerged rigid vegetation. In: Proceedings of the 35th IAHR world congress, Sept. 8–13, Chengdu, China

Tang, X., Rahimi, H., Singh, P., Wei, Z., Wang, Y., Zhao, Y. and Lu, Q. 2018. Experimental study of open-channel flow with partial double-layered vegetation. Proceedings of the 1st International Symposium on Water Resource and Environmental Management (WREM 2018), 1-7, ES3-22, Nov. 28-29, Kunming, China.

Tang, X. 2018a. Methods for predicting vertical velocity distributions in open channel flows with submerged rigid vegetation. In: Proceedings of the 21st IAHR-APD Congress, Vol.1, 567-576, Sept. 2–5, Yogyakarta, Indonesia.

Tang, X. 2018b. Evaluating methods for discharge prediction of straight asymmetric compound channels. Journal of Geological Resource and Engineering, 6(5):217-227, DOI: 10.17265/2328-2193.

Tang, X. 2019a. An improved analytical model for vertical velocity distribution of vegetated channel flows. Journal of Geoscience and Environment Protection, 7(4), 42-60, DOI:10.4236/gep.2019.74004.

Tang, X. 2019b. Evaluating two-layer models for velocity profiles in open-channels with submerged vegetation. Journal of Geoscience and Environment Protection, 7(1), 68-80, DOI: 10.4236/gep.2019.71006.

Tang, X. 2019c. A mixing-length-scale-based analytical model for predicting velocity profiles of open channel flows with submerged rigid vegetation." Water Environ J. 33(4), 610-619, https://doi.org/10.1111/wej.12434

Tang, X., Rahimi, H.R., Wang, Y., Zhao, Y., Lu, Q. Wei, Z. and Singh, P. 2019. Flow characteristics of open-channel flow with partial two-layered vegetation. Proceedings of the 38th IAHR World Congress, Sept. 1-6, 2019, Panama City, Panama.

Temple, D. M. 1986. Velocity distribution coefficients for grass-lined channels. Journal of Hydraulic Engineering, 112(3), 193-205.

Thom, A. S. 1971. Momentum absorption by vegetation. Quarterly Journal of the Royal Meteorological Society, 97(414), 414-428.

Tsujimoto, T., and Kitamura, T. 1990. Velocity profile of flow in vegetated-bed channels." KHL progressive report, 1.

744 Yilmazer, D., Ozan, A. Y., & Cihan, K. 2018. Flow Characteristics in the Wake Region of a
745 Finite-Length Vegetation Patch in a Partly Vegetated Channel. Water, 10(4), 459.